Single-photon manipulations based on optically controlled chiral couplings in waveguide structures of Rydberg giant atoms

Yao-Tong Chen,[1] Lei Du,[2] Zhihai Wang,[1] M. Artoni,[3,4,*] G. C. La Rocca,[5,†] and Jin-Hui Wu[1,‡]
[1]*School of Physics and Center for Quantum Sciences, Northeast Normal University, Changchun 130024, China*
[2]*Department of Microtechnology and Nanoscience, Chalmers University of Technology, 41296 Gothenburg, Sweden*
[3]*Department of Engineering and Information Technology, Brescia University, 25133 Brescia, Italy*
[4]*European Laboratory for Nonlinear Spectroscopy, 50019 Sesto Fiorentino, Italy*
[5]*NEST, Scuola Normale Superiore, 56126 Pisa, Italy*

(Received 19 December 2023; accepted 3 June 2024; published 25 June 2024)

Two interacting Rydberg atoms coupled to a waveguide may realize a giant-atom platform that exhibits controllable (phase-dependent) chirality through which the direction of nonreciprocally scattered photons can be switched on demand, e.g., by the geometrical tuning of an external driving field. In our platform, at variance with traditional setups, the chirality arises from a simple optical implementation of the local phase difference between two coupling points of the Rydberg giant atom. When employing two (or more) driving fields, this platform can also be used as a frequency converter with its strongly asymmetric efficiency being significantly enhanced via the chiral couplings. Our Rydberg giant-atom platform is well suited for chiral quantum optics applications and further offers direct scalability for reaching tunable frequency conversion in the optical domain.

DOI: 10.1103/PhysRevA.109.063710

I. INTRODUCTION

Rydberg atoms with large principal quantum numbers, combining long coherence times and strong long-range interactions, can serve as attractive building blocks for many important applications, including scalable quantum computing and long-distance quantum communication [1–3]. Note, in particular, that strong Rydberg interactions can well suppress multiple atomic excitations within a blockade radius by shifting the resonance of double atomic excitations [4], which opens possibilities to explore single-photon generation [5–7], quantum logic gates [8–10], entangled states [11–14], and quantum simulators [15,16]. Very recently, interacting Rydberg atoms have been considered as a new platform to implement actual giant-atom physics working in the optical domain, with peculiar self-interference effects and entanglement-onset dynamics [17]. It is then worth noting that giant atoms have emerged as a novel paradigm in quantum optics and are generally characterized by multiple couplings with electromagnetic or acoustic modes at distinct points, hence breaking the dipole approximation [18]. Experimental platforms of typical giant atoms are presently available including, e.g., superconducting quantum circuits [19–22], coupled waveguide arrays [23], and ferromagnetic spin systems [24].

Benefiting from diverse geometric structures owing to multiple coupling points between giant atoms and waveguide modes, rich interference effects can be introduced to modify relevant interactions, opening a broad field of perspectives for controlling photon transport and information processing. A series of unique characteristics, e.g., frequency-dependent atomic relaxation rates and Lamb shifts [25–27], nonexponential atomic decay [20,28], in-band decoherence-free interactions [21,29–31], and long-lived entanglement generation [32], have already been discovered in different giant-atom schemes. Especially, for some chiral setups based on giant atoms, unlike others based on spin-momentum locking effect [33–35] or topological waveguides [36,37], the direction-dependent couplings can be realized by introducing a local coupling-phase difference to break the time-reversal symmetry, resulting in chiral spontaneous emission and nonreciprocal transmission [38–41]. Considering specifically designed multilevel atomic structures in waveguide quantum electrodynamics systems, more abundant behaviors of photon scattering will appear, including asymmetric photon routing [42,43] or circulating [44,45], and efficient frequency conversion [46–49].

This paper aims at tackling a few issues of the optical giant-atom physics using Rydberg atoms, building upon our earlier work [17]. We extend this work to encompass scenarios involving multiple drivings and chiral couplings to attain on demand nonreciprocal light scattering and asymmetric frequency conversion. In Sec. II, we consider the basic case of two two-level Rydberg atoms coupled to one waveguide mode and driven by one external field (see Fig. 1). In an appropriate regime, both single-excitation states remain unpopulated and can be adiabatically eliminated, leading to an equivalent giant atom coupled to the waveguide mode at two points. Scattering properties of this giant atom are sensitive to the relative phase of two waveguide-atom coupling coefficients and also controlled by the driving field's angle of incidence, thus yielding tunable nonreciprocal transmissivities.

*Contact author: maurizio.artoni@unibs.it
†Contact author: giuseppe.larocca@sns.it
‡Contact author: jhwu@nenu.edu.cn

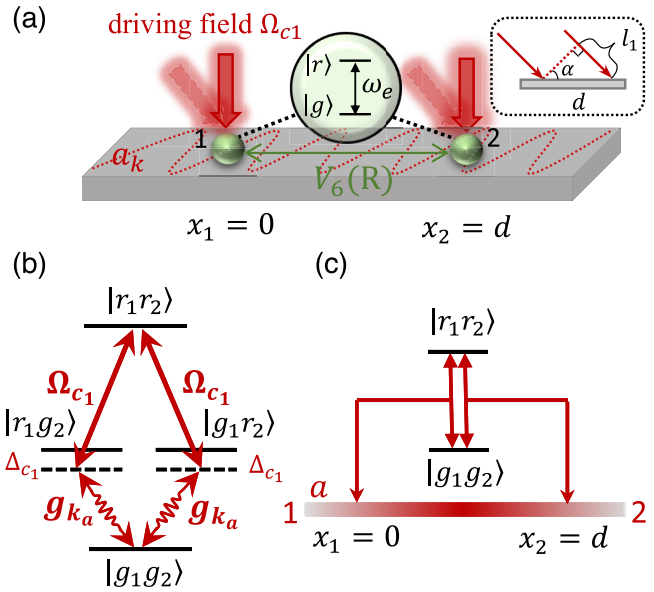

FIG. 1. Schematic diagram for achieving nonreciprocal transmission of one waveguide mode. (a) Two two-level Rydberg atoms interacting via a vdW potential V_6, coupled to a waveguide mode a respectively at $x_1 = 0$ and $x_2 = d$, and driven by a coherent field Ω_{c1}. If the driving field is oblique with angle α, there will be a phase difference as it reaches the two atoms ascribed to optical path difference l_1 (see the inset). (b) The four-level configuration in the two-atom basis where driving field Ω_{c1} is matched in frequency with waveguide mode a on both left and right paths of two-photon resonance. (c) The equivalent two-level giant atom exhibiting two coupling points when adiabatically eliminating two single-excitation states.

In Sec. III, we consider another case in which different Rydberg atoms are driven by different external fields matching different waveguide modes in frequency under the two-photon resonance (see Fig. 4). While this nonlocal system with each waveguide mode exhibiting one coupling point no longer mimics a giant atom, and hence exhibits reciprocal scattering properties, it may operate as a symmetric frequency converter whereby a photon propagating in one waveguide mode, independent of its input port, can be converted into a photon propagating in the other waveguide mode and vice versa. In Sec. IV, we consider the more complex case in which both Rydberg atoms are driven by two external fields and coupled to two waveguide modes with matched frequencies under the two-photon resonance (see Fig. 6). This nonlocal system with each waveguide mode exhibiting two coupling points behaves as a giant atom again and becomes sensitive to the two relative phases of the four waveguide-atom coupling coefficients. Its frequency conversion properties can be made highly asymmetric and more efficient, e.g., by changing the angle of incidence of each driving field.

II. NONRECIPROCAL TRANSMISSION

We consider two identical atoms 1 and 2 with resonant transition frequency ω_e and intrinsic dissipation rate γ (into the free space) from Rydberg state $|r\rangle$ to ground state $|g\rangle$. They are driven by a coherent field with Rabi frequency Ω_{c1} and coupled to a photonic crystal waveguide at $x_1 = 0$ and $x_2 = d$, respectively, as shown in Fig. 1(a). They also interact via a van der Waals (vdW) potential $V_6 = C_6/R^6$ [1], where C_6 and R are the vdW coefficient and the interatomic distance, respectively. This potential shifts the frequency of double-excitation state $|r_1r_2\rangle$ from $2\omega_e$ to $2\omega_e + V_6$ yet without affecting the frequency ω_e of single-excitation states $|r_1g_2\rangle$ and $|g_1r_2\rangle$. The driving field is assumed to exhibit a frequency ω_{c1} close to $\omega_e + V_6$ but sufficiently far detuned from ω_e. We further assume that $\omega_e + V_6$ falls within a band gap of the waveguide, while ω_e corresponds to a propagating waveguide mode a. Then, the two upper transitions $|r_1g_2\rangle \to |r_1r_2\rangle$ and $|g_1r_2\rangle \to |r_1r_2\rangle$ only couple with the driving field Ω_{c1}, while the two lower transitions $|g_1g_2\rangle \to |r_1g_2\rangle$ and $|g_1g_2\rangle \to |g_1r_2\rangle$ only couple with the waveguide mode a. Based on all above considerations, as done in our recent work [17], we can obtain a four-level configuration in the two-atom basis as shown in Fig. 1(b) where the detuning $\Delta_{c1} = \omega_{c1} - (\omega_e + V_6)$ is restricted by $|\Delta_{c1}| \ll V_6$ and the resonance condition on two-photon transition $|g_1g_2\rangle \to |r_1r_2\rangle$ can be satisfied for a matching waveguide-mode frequency $\omega_e - \Delta_{c1}$.

The system Hamiltonian, under the rotating-wave approximation, can be written as ($\hbar = 1$)

$$\begin{aligned} H_{A_k} &= (\omega_e - i\gamma)(|g_1r_2\rangle\langle g_1r_2| + |r_1g_2\rangle\langle r_1g_2|) \\ &\quad + (2\omega_e + V_6 - 2i\gamma)|r_1r_2\rangle\langle r_1r_2| + \int dk_a \omega_{ka} a_k^\dagger a_k \\ &\quad + \left[\int g_a dk_a a_k (|r_1g_2\rangle\langle g_1g_2| + |g_1r_2\rangle\langle g_1g_2| e^{ik_a d}) \right. \\ &\quad \left. + \Omega_{c1} e^{-i\omega_{c1}t}(|r_1r_2\rangle\langle r_1g_2| + e^{i\theta_1}|r_1r_2\rangle\langle g_1r_2|) + \text{H.c.}\right]. \end{aligned} \tag{1}$$

Here, a_k ($a_k^\dagger$) refers to the bosonic annihilation (creation) operators of waveguide mode a denoted by wave vector k_a and frequency ω_{ka}; θ_1 represents the phase difference between two Rabi frequencies of a common magnitude Ω_{c1} for different atoms, which is easily controlled by utilizing an oblique driving field with angle α deviating from the normal to the waveguide. To be more concrete, we have $\theta_1 = k_{c1} l_1$ where k_{c1} is the wave vector of the driving field and $l_1 = d \sin\alpha$ is the optical path difference between the two driving points (being $\theta_1 = 0$ when the field is incident normally). Under the Weisskopf-Wigner approximation, we further have a constant coupling strength $g_{ka} = g_a$ for the waveguide modes of frequencies $\omega_{ka} \simeq \omega_e$ and a constant atomic decay rate $\Gamma_a = g_a^2/v_g$ into these waveguide modes with v_g being the group velocity of waveguide photons. The present model differs from that in [17] for an extra relative phase θ_1, which would bring equivalent chiral couplings into play as discussed later.

Above, we have first provided Hamiltonian H_{A_k} in the momentum space because it allows for an exact description of the present model and is also indispensable for deriving the conditions under which a four-level Rydberg pair can be regarded as a two-level giant atom (see Appendix A). To investigate the scattering of a single waveguide photon by two interacting Rydberg atoms initially in the ground state

$|g_1g_2\rangle$, however, it is more convenient to employ the approach developed by Shen and Fan [50,51], used in [39,49,52,53], and referred to as the Bethe-ansatz approach [54]. This approach requires, in particular, the real-space Hamiltonian

$$H_{A_x} = (\omega_e - i\gamma)(|r_1g_2\rangle\langle r_1g_2| + |g_1r_2\rangle\langle g_1r_2|) + (2\omega_e + V_6 - 2i\gamma)|r_1r_2\rangle\langle r_1r_2| + \int_{-\infty}^{+\infty} dx\Big[a_L'^{\dagger}(x)\Big(\omega_0 + iv_g\frac{\partial}{\partial x}\Big)a_L'(x) + a_R'^{\dagger}(x)\Big(\omega_0 - iv_g\frac{\partial}{\partial x}\Big)a_R'(x)\Big] + \int_{-\infty}^{+\infty} dx\{\delta(x)g_a[a_R(x) + a_L(x)]|r_1g_2\rangle\langle g_1g_2| + \delta(x-d)g_a[a_R(x) + a_L(x)]|g_1r_2\rangle\langle g_1g_2| + \text{H.c.}\} + \Omega_{c1}e^{-i\omega_{c1}t}(|r_1r_2\rangle\langle r_1g_2| + e^{i\theta_1}|r_1r_2\rangle\langle g_1r_2|) + \text{H.c.} \tag{2}$$

obtained from H_{A_k} via a standard Fourier transform [51]. Here, $a_L = a_L'e^{-ik_0x}$ ($a_L^{\dagger} = a_L'^{\dagger}e^{ik_0x}$) and $a_R = a_R'e^{ik_0x}$ ($a_R^{\dagger} = a_R'^{\dagger}e^{-ik_0x}$) denote the annihilation (creation) operators of left-going and right-going photons in waveguide mode a, respectively, with a_L' and a_R' representing spatially slowly varying envelopes. Note also that the delta functions $\delta(x)$ and $\delta(x-d)$ describe two spatially separated coupling points, and we have chosen $\omega_0 = \omega_e$ as the frequency around which the dispersion relation of waveguide mode a can be linearized as $\omega_{ka} = \omega_0 - (k_0 \pm k_a)v_g$ with "+" ("−") referring to the left (right) branch. For a waveguide photon of central frequency ω_{ka} (its detuning is defined as $\delta_{ka} = \omega_{ka} - \omega_e$) incident from port 1 on the left or from port 2 on the right, one can solve the stationary Schrödinger equation $H_{A_x}|\Psi_{A_x}\rangle = \omega_{ka}|\Psi_{A_x}\rangle$ to examine the eigenstate

$$|\Psi_{A_x}\rangle = \int_{-\infty}^{+\infty} dx\big[\Phi_{aR}^A(x)a_R^{\dagger}(x) + \Phi_{aL}^A(x)a_L^{\dagger}(x)\big]|0, g_1g_2\rangle + u_b^A|0, r_1g_2\rangle + u_c^A|0, g_1r_2\rangle + u_d^A|0, r_1r_2\rangle, \tag{3}$$

where $|0, g_1g_2\rangle$ denotes the vacuum state of the system without waveguide photons and excited atoms; u_b^A, u_c^A, and u_d^A are the excitation probability amplitudes of different atomic states. Note that all terms in $|\Psi_{A_x}\rangle$ belong to the single-excitation subspace of waveguide photons, as the double-excitation state $|r_1r_2\rangle$ corresponds to a two-photon transition from the ground state $|g_1g_2\rangle$ in which only one quantum of the waveguide mode is exchanged (the other comes from the driving field).

Moreover, under appropriate boundary conditions, the densities of probability amplitudes for right-going and left-going photons can be written respectively as

$$\Phi_{aR}^A(x) = e^{ik_ax}\{\Theta(-x) + A_1[\Theta(x) - \Theta(x-d)] + t_{1\to2}\Theta(x-d)\},$$
$$\Phi_{aL}^A(x) = e^{-ik_ax}\{r_{1\to1}\Theta(-x) + A_2[\Theta(x) - \Theta(x-d)]\}, \tag{4}$$

referring to the case where one photon is incident from the left (i.e., port 1) of the waveguide, or

$$\Phi_{aR}^A(x) = e^{ik_ax}\{A_3[\Theta(x) - \Theta(x-d)] + r_{2\to2}\Theta(x-d)\},$$
$$\Phi_{aL}^A(x) = e^{-ik_ax}\{\Theta(x-d) + A_4[\Theta(x) - \Theta(x-d)] + t_{2\to1}\Theta(-x)\}, \tag{5}$$

referring to the case where one photon is incident from the right (i.e., port 2) of the waveguide. Above, we have used $A_{1,3}$ ($A_{2,4}$) to denote the probability amplitudes for a right-going (left-going) photon within the region of $0 < x < d$, while $\Theta(x)$ is the Heaviside step function with $\Theta(x) = 0$ for $x < 0$, $\Theta(x) = 1/2$ for $x = 0$, and $\Theta(x) = 1$ for $x > 0$, using the half-maximum convention [55]. All unknown coefficients appearing in $|\Psi_{A_x}\rangle$ can be obtained straightforwardly (see Appendix A1) from the solution of $H_{A_x}|\Psi_{A_x}\rangle = \omega_{ka}|\Psi_{A_x}\rangle$, This then yields two transmissivities $T_{1\to2} = |t_{1\to2}|^2$ and $T_{2\to1} = |t_{2\to1}|^2$, which are in general different (i.e., nonreciprocal) due to equivalent giant-atom chiral couplings as discussed below.

A. Equivalent giant atom

Under the two-photon resonance condition (i.e., $\Delta_{c1} + \delta_{ka} \simeq 0$) and with detunings much larger than coupling strengths (i.e., $|\delta_{ka}| \simeq |\Delta_{c1}| \gg \Omega_{c1}, g_a$), it has been shown that the double-excitation state $|r_1r_2\rangle$ decays directly to the ground state $|g_1g_2\rangle$, exhibiting a giant-atom self-interference behavior [17]. Now we try to show that the scattering properties of two Rydberg atoms can also be equivalent to those of a giant atom under the same considerations. For this purpose, we assume that both atoms are initially at state $|g_1g_2\rangle$ and will be excited to state $|r_1r_2\rangle$ directly by a waveguide-mode photon and a driving-field photon together, leaving the single-excitation states $|r_1g_2\rangle$ and $|g_1r_2\rangle$ almost unpopulated during the scattering process. Then, one can adiabatically eliminate states $|r_1g_2\rangle$ and $|g_1r_2\rangle$ [56,57] and obtain the *effective* momentum-space Hamiltonian $H_{A_k}^{\text{eff}}$ of a two-level giant-atom as shown in Fig. 1(c) from the *original* momentum-space Hamiltonian H_{A_k} (see Appendix A2). With $H_{A_k}^{\text{eff}}$ in hand, it is straightforward to obtain the *effective* real-space Hamiltonian [51]

$$H_{A_x}^{\text{eff}} = \Big(2\omega_e + V_6 - \frac{2\Omega_{c1}^2}{\Delta_{c1}} - 2i\gamma\Big)|r_1r_2\rangle\langle r_1r_2| + \int_{-\infty}^{+\infty} dx\Big[a_L'^{\dagger}(x)\Big(\omega_{c1} + \omega_0 + iv_g\frac{\partial}{\partial x}\Big)a_L'(x) + a_R'^{\dagger}(x)\Big(\omega_{c1} + \omega_0 - iv_g\frac{\partial}{\partial x}\Big)a_R'(x)\Big] + \Big\{\int_{-\infty}^{+\infty} dx\xi_a[a_R(x) + a_L(x)]|r_1r_2\rangle\langle g_1g_2|[\delta(x) + \delta(x-d)e^{i\theta_1}] + \text{H.c.}\Big\}, \tag{6}$$

where $2\Omega_{c1}^2/\Delta_{c1}$ is the effective energy shift of state $|r_1 r_2\rangle$ and $\xi_a = -g_a\Omega_{c1}/\Delta_{c1}$ is the effective coupling strength of relevant two-photon transition processes.

Again, the eigenstate of $H_{A_x}^{\rm eff}|\tilde{\Psi}_{A_x}\rangle = (\omega_{ka}+\omega_{c1})|\tilde{\Psi}_{A_x}\rangle$ can be written as (Bethe-ansatz approach)

$$|\tilde{\Psi}_{A_x}\rangle = \int_{-\infty}^{+\infty} dx\big[\tilde{\Phi}_{aR}^{A}(x)a_R^\dagger(x) + \tilde{\Phi}_{aL}^{A}(x)a_L^\dagger(x)\big]|0, g_1 g_2\rangle + \tilde{u}_d^A|0, r_1 r_2\rangle, \tag{7}$$

where $\tilde{\Phi}_{aL}^{A}$, $\tilde{\Phi}_{aR}^{A}$, and $\tilde{u}_d^A$ have similar physical meanings as Φ_{aL}^{A}, Φ_{aR}^{A}, and u_d^A in Eq (3), respectively. Then, for a photon of central frequency ω_{ka} incident from port 1 or port 2 of the waveguide, one can obtain the analytical expressions of transmissivities $T_{1\to2}^{\rm eff} = |t_{1\to2}^{\rm eff}|^2$ and $T_{2\to1}^{\rm eff} = |t_{2\to1}^{\rm eff}|^2$ (see Appendix A1) as

$$T_{1\to2}^{\rm eff} = \left|\frac{\delta_{\rm tot}+2i\gamma-2\Upsilon_a e^{i\theta_1}\sin\phi_a}{\delta_{\rm tot}+2i\gamma+2i\Upsilon_a(1+e^{i\phi_a}\cos\theta_1)}\right|^2,$$
$$T_{2\to1}^{\rm eff} = \left|\frac{\delta_{\rm tot}+2i\gamma-2\Upsilon_a e^{-i\theta_1}\sin\phi_a}{\delta_{\rm tot}+2i\gamma+2i\Upsilon_a(1+e^{i\phi_a}\cos\theta_1)}\right|^2, \tag{8}$$

with $\delta_{\rm tot} = \delta_{ka}+\Delta_{c1}+2\Omega_{c1}^2/\Delta_{c1}$ denoting the total two-photon detuning, $\Upsilon_a = \xi_a^2/v_g$ the decay rate into waveguide mode a at each coupling point, and $\phi_a = k_a d$ the phase accumulated between two coupling points that can be taken as constant in the Markovian regime [39]. In this subsection, we wish to test the validity of adiabatically eliminating two single-excitation states, and first focus on the *nonchiral* case of a normal driving field's incidence ($\theta_1 = 0$) corresponding to a reciprocal transmission with $T^{\rm eff} = T_{1\to2}^{\rm eff} = T_{2\to1}^{\rm eff}$ and $T = T_{1\to2} = T_{2\to1}$.

Comparing the spectra of transmissivities T from the four-level double-atom model and $T^{\rm eff}$ from the two-level giant-atom model in Figs. 2(a)–2(c) for different values of Δ_{c1}, it is clear that T and $T^{\rm eff}$ become closer and closer as Δ_{c1} increases, indicating that the adiabatic elimination becomes more and more reliable. At the same time, we note that $\Upsilon_a = \Gamma_a\Omega_{c1}^2/\Delta_{c1}^2$ becomes smaller for larger Δ_{c1}, which causes the minimum values of T and $T^{\rm eff}$, represented by a dip around $\delta_{ka} \simeq -\Delta_{c1}$, to increase. In particular, we find that the two-level giant-atom model is very accurate at $\Delta_{c1} = 30\Gamma_a$, for which we have plotted T ($T^{\rm eff}$) against detuning δ_{ka} and phase ϕ_a in Fig. 2(d) to show the typical phase-dependent transmission spectra of a giant atom. It is also worth noting that $T^{\rm eff}(T) \equiv 1$ with $\phi_a = (2n+1)\pi$ (n is an integer) refers to the specific case of two Rydberg atoms equivalent to a giant atom being decoupled from the waveguide mode. The above findings can find appropriate explanations from Eq. (8). For instance, the phase-dependent transmission spectra can be attributed to the overall Lamb shift $-2\Upsilon_a\cos\theta_1\sin\phi_a$ and decay rate $2\Upsilon_a(1+\cos\theta_1\cos\phi_a)$ as induced by waveguide mode a and controlled by the driving field. Such a periodic phase modulation depending also on Δ_{c1} and Ω_{c1} through Υ_a occurs due to *two-path interference effects* arising from the giant-atom two-point couplings. That is, a left-incident photon accumulates the phase ϕ_a when traveling directly from $x_1 = 0$ to $x_2 = d$, or acquires the phase $-\theta_1$ when absorbed (emitted) at $x_1 = 0$ ($x_2 = d$) together with a driving field photon. The self-interference of a photon between the direct path (ϕ_a) and the indirect path ($-\theta_1$) then results in above phase-dependent Lamb shift and decay rate. Similarly, for a right-incident photon, it accumulates again the phase ϕ_a when traveling directly from $x_2 = d$ to $x_1 = 0$, but acquires a reversed phase θ_1 when absorbed (emitted) at $x_2 = d$ ($x_1 = 0$).

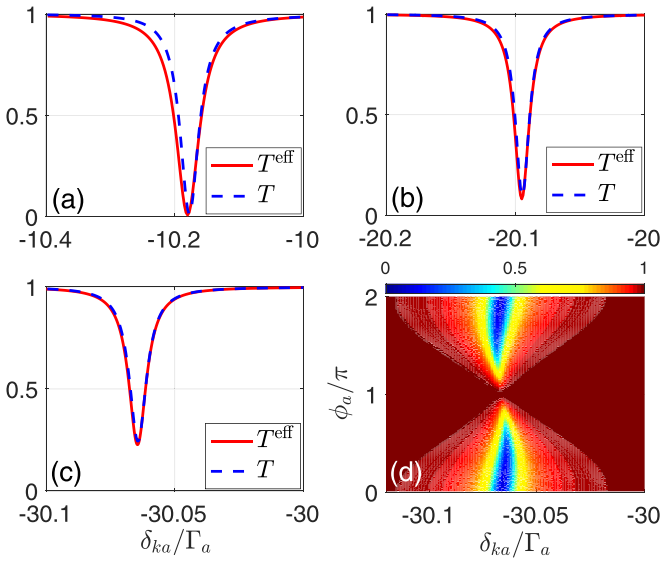

FIG. 2. Reciprocal transmissivities T and $T^{\rm eff}$ vs detuning δ_{ka} with $\phi_a = (2n+1/2)\pi$ and (a) $\Delta_{c1} = 10\Gamma_a$, (b) $\Delta_{c1} = 20\Gamma_a$, and (c) $\Delta_{c1} = 30\Gamma_a$. (d) Reciprocal transmissivity T ($T^{\rm eff}$) vs detuning δ_{ka} and phase ϕ_a (modulo 2π) with $\Delta_{c1} = 30\Gamma_a$. Other parameters are taken as $\theta_1 = 2n\pi$, $\gamma = 10^{-3}\Gamma_a$, $\Omega_{c1} = \Gamma_a$, $V_6 = 2\times10^4\Gamma_a$, and $\Gamma_a = 1$ MHz.

B. Equivalent chiral couplings

It is now worth recalling that coupling phases may be introduced, e.g., through Josephson-junction loops when threaded by external fluxes [38] or through a dissipation port at the coupling point [41] in superconducting quantum systems. Here, we present a much simpler method to realize chiral couplings in the optical domain based on our Rydberg giant-atom platform, where the chirality is attained by controlling the nonvanishing local phase difference θ_1 between two coupling points of the equivalent giant atom [38–40]. Directly adjusting the incident angle α of an oblique driving field would then enable one, in the presence of intrinsic atomic dissipation ($\gamma \neq 0$), to realize the nonreciprocal transmission.

We plot in Figs. 3(a)–3(c) relevant transmissivities against detuning δ_{ka} when a waveguide photon is incident from port 1 on the left or from port 2 on the right in the case of perfect chiral couplings with $\phi_a = (2n+1/2)\pi$ and $\theta_1 = (2n+1/2)\pi$. It is clear that, around the two-photon resonance $\delta_{ka} \simeq -\Delta_{c1}$, transmissivities $T_{1\to2}$ and $T_{1\to2}^{\rm eff}$ from port 1 to port 2 (or $T_{2\to1}$ and $T_{2\to1}^{\rm eff}$ from port 2 to port 1) are very different for different values of Δ_{c1}. That is because, other than determining the validity of adiabatically eliminating two single-excitation states [the same conclusion is depicted in Figs. 2(a)–2(c)], a change of Δ_{c1} will result in different values of the waveguide decay rate Υ_a while the intrinsic dissipation rate γ remains fixed. For instance, in Fig. 3(c), we can observe $T_{1\to2} \simeq T_{1\to2}^{\rm eff} \simeq 0$ ($T_{2\to1} \simeq T_{2\to1}^{\rm eff} \equiv 1$) at the resonance point when Υ_a and

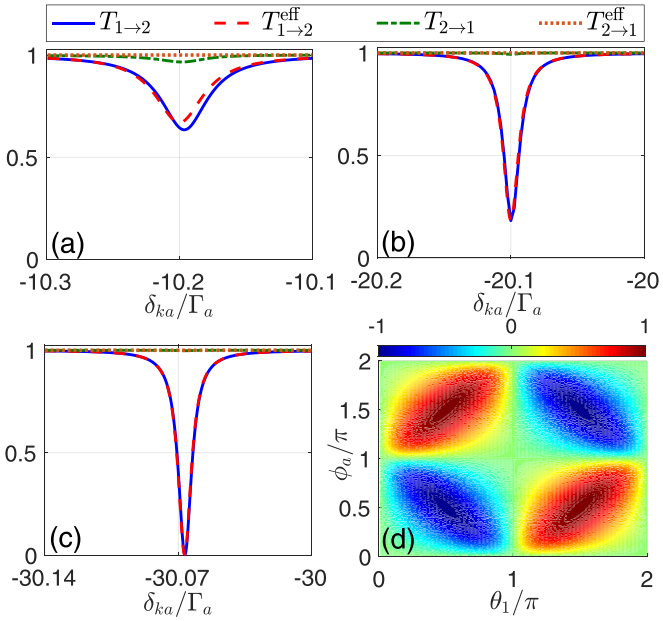

FIG. 3. Nonreciprocal transmissivities $T_{1\to2}$ and $T_{2\to1}$ as well as $T^{\rm eff}_{1\to2}$ and $T^{\rm eff}_{2\to1}$ vs detuning δ_{ka} with $\phi_a=\theta_1=(2n+1/2)\pi$ and (a) $\Delta_{c1}=10\Gamma_a$, (b) $\Delta_{c1}=20\Gamma_a$, and (c) $\Delta_{c1}=30\Gamma_a$. (d) Transmission contrast ratio I vs phases θ_1 (modulo 2π) and ϕ_a (modulo 2π) with $\delta_{ka}=-30.067\Gamma_a$ and $\Delta_{c1}=30\Gamma_a$. Other parameters are the same as in Fig. 2.

γ are almost the same. Therefore, with the experimentally reasonable parameters of Υ_a used here, Rydberg atoms are most suitable to realize perfect nonreciprocal transmission due to the fact that their intrinsic dissipations are about two orders smaller compared with those of typical atoms [58–60]. Furthermore, the transmission contrast ratio

$$I=\frac{T_{2\to1}-T_{1\to2}}{T_{2\to1}+T_{1\to2}}, \tag{9}$$

plotted in Fig. 3(d), shows that the transmission nonreciprocity due to the chiral couplings can be easily tuned by the relative phases θ_1 and ϕ_a.

It is worth noting that γ plays a crucial role in the nonreciprocal transmission and we have $I\equiv0$ when neglecting γ [39]. This decay rate may increase a few times when two Rydberg atoms are close to the waveguide [61], but its detrimental effects can by mitigated by employing stronger driving fields. Let us start by considering left- and right-incident photons together; they are scattered differently in general, with $t^{\rm eff}_{1\to2}\neq t^{\rm eff}_{2\to1}$, due to different interplay of phases ϕ_a and $\pm\theta_1$ in the numerators of $t^{\rm eff}_{1\to2}$ and $t^{\rm eff}_{2\to1}$ in Eq. (8), which we now rearrange as

$$\begin{aligned}&\delta_{\rm tot}-2\Upsilon_a\cos\theta_1\sin\phi_a+i(2\gamma-2\Upsilon_a\sin\theta_1\sin\phi_a),\\&\delta_{\rm tot}-2\Upsilon_a\cos\theta_1\sin\phi_a+i(2\gamma+2\Upsilon_a\sin\theta_1\sin\phi_a).\end{aligned} \tag{10}$$

It shows that, only when $\gamma=0$, left-incident and right-incident photons exhibit the same transmittivity $T^{\rm eff}_{1\to2}=T^{\rm eff}_{2\to1}$, though they experience different *two-path interference effects* described by $\pm\theta_1$ of the driving field. When $\gamma\neq0$, however, the numerators of $t^{\rm eff}_{1\to2}$ and $t^{\rm eff}_{2\to1}$ are different in their imaginary parts, not by sign but by magnitude, so that we must have $T^{\rm eff}_{1\to2}\neq T^{\rm eff}_{2\to1}$. In particular, left-incident photons are not transmitted with $T^{\rm eff}_{1\to2}=0$ ($I=1$) in the case of $\delta_{\rm tot}=2\Upsilon_a\cos\theta_1\sin\phi_a$ and $\gamma=\Upsilon_a\sin\theta_1\sin\phi_a$, while right-incident photons are not transmitted with $T^{\rm eff}_{2\to1}=0$ ($I=-1$) in the case of $\delta_{\rm tot}=2\Upsilon_a\cos\theta_1\sin\phi_a$ and $\gamma=-\Upsilon_a\sin\theta_1\sin\phi_a$. More specifically, at the resonance ($\delta_{\rm tot}=0$), nonreciprocal transmission ($I=\pm1$) occurs for $\theta_1=(2n+1/2)\pi$ and $\gamma=\pm\Upsilon_a\sin\phi_a$ or $\theta_1=(2n-1/2)\pi$ and $\gamma=\mp\Upsilon_a\sin\phi_a$, while reciprocal transmission ($I=0$) occurs for $\theta_1=(2n+1)\pi$ or $\phi_a=(2n+1)\pi$, in agreement with Fig. 3(d).

We finally discuss suitable experimental parameters by considering ground state $|g_{1,2}\rangle=|5S_{1/2},F=2,m_F=2\rangle$ and Rydberg state $|r_{1,2}\rangle=|75P_{3/2},m_J=3/2\rangle$ for two ^{87}Rb atoms, exhibiting transition frequency $\omega_e\simeq2\pi\times1009\,$THz, intrinsic lifetime $\tau\simeq964\,\mu$s ($\gamma\simeq1.0\,$kHz), and vdW coefficient $C_6\simeq2\pi\times2.8\times10^{12}\,{\rm s}^{-1}\mu{\rm m}^6$ [17]. Thus, we have $R=\sqrt[6]{C_6/V_6}\simeq3.1\,\mu$m for $V_6\simeq20\,$GHz corresponding to $\phi_a=k_ad\simeq20.7\pi$ in the case of $R=d$ and $|\delta_{ka}|\ll V_6\ll\omega_e$. Keeping R and hence V_6 invariant, we can use optical tweezers [62] to change d in the xy plane from 2.8 to 3.1 μm for a misalignment within the range $[25.4^\circ,0^\circ]$ to gain a 2π modulation of ϕ_a. Considering that $\theta_1\simeq\phi_a\sin\alpha$ obtained with $\omega_{c1}\simeq\omega_{ka}\simeq\omega_e$ depends on both ϕ_a and α, it is impossible to determine α for a given θ_1 when we vary ϕ_a as in Fig. 3(d). Hence, we stress here that θ_1 can be tuned from 6π to 8π for $\alpha\in[16.8^\circ,25.3^\circ]$ in the case of $\phi_a\in[18.7\pi,20.7\pi]$. Note also that α is tuned in the xz plane and its change has no influences on the misalignment in the xy plane. Similar remarks hold for the relation between phase θ_2 and angle β of a second driving field, as discussed below.

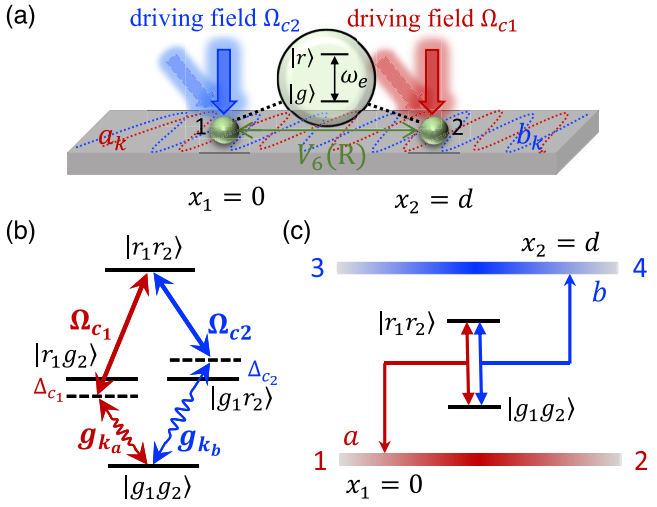

FIG. 4. Schematic diagram for achieving symmetric frequency conversion between two waveguide modes. (a) The same waveguide-coupled Rydberg-atom platform as in Fig. 1(a) except atoms 1 and 2 are driven by coherent fields Ω_{c1} and Ω_{c2} at different incident angles, respectively. (b) The four-level configuration in the two-atom basis where driving field Ω_{c1} (Ω_{c2}) is matched in frequency with waveguide mode a (b) on the left (right) path of two-photon resonance. (c) The equivalent two-level nonlocal atom coupled to each waveguide mode at one point when eliminating two single-excitation states.

Since the spatial extents of highly excited Rydberg states may compare with the optical wavelengths of both driving fields and waveguide modes, the issue of continuous couplings, rather than pointlike couplings, should be considered. But, we can verify through a dynamical solution method in the momentum space (see Appendix A3) that the nonreciprocal transmission is robust since all results found above remain essentially quantitatively unchanged even for continuous couplings.

III. SYMMETRIC FREQUENCY CONVERSION

In addition to realizing nonreciprocal transmission for one waveguide mode, another possible application of our Rydberg-atom platform is to attain frequency conversion between two waveguide modes. This can be implemented by applying coherent fields Ω_{c1} and Ω_{c2} with frequencies ω_{c1} and ω_{c2} upon atoms 1 and 2, respectively, as shown in Fig. 4(a). If we further assume $|\omega_{c1}-\omega_{c2}| \gg \Omega_{c1,c2}$, each atom will couple to a different waveguide mode (a or b), rather than the same waveguide mode (a) as shown in Fig. 1(a), under the two-photon resonance from ground state $|g_1g_2\rangle$ to double-excitation state $|r_1r_2\rangle$. This then results in the four-level configuration in the two-atom basis as shown in Fig. 4(b), whereby driving field Ω_{c1} and waveguide mode a form the left path while driving field Ω_{c2} and waveguide mode b form the right path. Accordingly, the system Hamiltonian can be written as

$$H_{B_k} = (\omega_e - i\gamma)(|g_1r_2\rangle\langle g_1r_2| + |r_1g_2\rangle\langle r_1g_2|) + (2\omega_e + V_6 - 2i\gamma)|r_1r_2\rangle\langle r_1r_2| + \int dk_a\omega_{ka}a_k^\dagger a_k + \int dk_b\omega_{kb}b_k^\dagger b_k$$
$$+\left[\int dk_a g_a a_k|r_1g_2\rangle\langle g_1g_2| + \int dk_b g_b b_k|g_1r_2\rangle\langle g_1g_2|e^{ik_bd} + \Omega_{c1}e^{-i\omega_{c1}t}|r_1r_2\rangle\langle r_1g_2| + \Omega_{c2}e^{-i\omega_{c2}t}e^{i\theta_2}|r_1r_2\rangle\langle g_1r_2| + \text{H.c.}\right], \tag{11}$$

where $b_k^\dagger$ (b_k) is the bosonic creation (annihilation) operators of the second waveguide mode with frequency ω_{kb} and wave vector k_b; g_b is the constant coupling strength between atom 2 and waveguide mode b and we will assume $g_b = g_a$ for simplicity; $\theta_2 = k_{c2}l_2$ is the phase difference with respect to optical path difference $l_2 = d\sin\beta$ for the second driving field at incident angle β. Transferring H_{B_k} in the momentum space into H_{B_x} in the real space, one can calculate scattering possibilities and conversion efficiencies of a right-going or left-going photon in waveguide mode a by solving the stationary Schrödinger equation as done in the last section for H_{A_x}.

In a similar way, adiabatically eliminating the single-excitation states $|r_1g_2\rangle$ and $|g_1r_2\rangle$, one can obtain the effective real-space Hamiltonian from its momentum space representation (see Appendix B) as

$$H_{B_x}^{\text{eff}} = \left(2\omega_e + V_6 - \frac{\Omega_{c1}^2}{\Delta_{c1}} - \frac{\Omega_{c2}^2}{\Delta_{c2}} - 2i\gamma\right)|r_1r_2\rangle\langle r_1r_2| + \int_{-\infty}^{+\infty} dx\left[a_L'^\dagger(x)\left(\omega_{c1}+\omega_0+iv_g\frac{\partial}{\partial x}\right)a_L'(x)\right.$$
$$\left.+ a_R'^\dagger(x)\left(\omega_{c1}+\omega_0-iv_g\frac{\partial}{\partial x}\right)a_R'(x)\right] + \int_{-\infty}^{+\infty} dx\left[b_L'^\dagger(x)\left(\omega_{c2}+\omega_0+iv_g\frac{\partial}{\partial x}\right)b_L'(x) + b_R'^\dagger(x)\left(\omega_{c2}+\omega_0-iv_g\frac{\partial}{\partial x}\right)b_R'(x)\right]$$
$$+\int_{-\infty}^{+\infty} dx\{\xi_a[a_R(x)+a_L(x)]|r_1r_2\rangle\langle g_1g_2|\delta(x) + \xi_b[b_R(x)+b_L(x)]|r_1r_2\rangle\langle g_1g_2|\delta(x-d)e^{i\theta_2} + \text{H.c.}\}, \tag{12}$$

with $\Delta_{c2} = \omega_{c2} - (\omega_e + V_6)$ and $\xi_b = -g_b\Omega_{c2}/\Delta_{c2}$. Here, $b_L = b_L'e^{-ik_0x}$ ($b_L^\dagger = b_L'^\dagger e^{ik_0x}$) and $b_R = b_R'e^{ik_0x}$ ($b_R^\dagger = b_R'^\dagger e^{-ik_0x}$) denote the annihilation (creation) operators of left-going and right-going photons in waveguide mode b, respectively. This Hamiltonian refers to an effective two-level system as shown in Fig. 4(c) that should be regarded as a nonlocal atom (but not a giant atom) since each of the two involved waveguide modes exhibits a single coupling point, thus yielding no self-interference effect. Its eigenstate can be written as

$$|\tilde{\Psi}_{B_x}\rangle = \int_{-\infty}^{+\infty} dx\left[\tilde{\Phi}_{aR}^B(x)a_R^\dagger(x) + \tilde{\Phi}_{aL}^B(x)a_L^\dagger(x) + \tilde{\Phi}_{bR}^B(x)b_R^\dagger(x)\right.$$
$$\left.+\tilde{\Phi}_{bL}^B(x)b_L^\dagger(x)\right]|0, g_1g_2\rangle + \tilde{u}_d^B|0, r_1r_2\rangle, \tag{13}$$

where $\tilde{\Phi}_{aR,aL}^B(x)$ and $\tilde{\Phi}_{bR,bL}^B(x)$ describe the densities of probability amplitudes for a right-going or left-going photon in waveguide modes a and b, respectively.

In this case, for example, if a single photon is incident from port 1 or port 2 of waveguide mode a, two ground-state Rydberg atoms will make a two-photon transition to the double-excitation state, simultaneously extracting another photon from the first driving field Ω_{c1}. Then, they will relax back to the ground state, emitting a photon into the other waveguide mode b along with another photon into the second driving field Ω_{c2}, or a photon into the original waveguide mode a along with another photon into the first driving field Ω_{c1}. Based on the Bethe-ansatz approach, one has (see

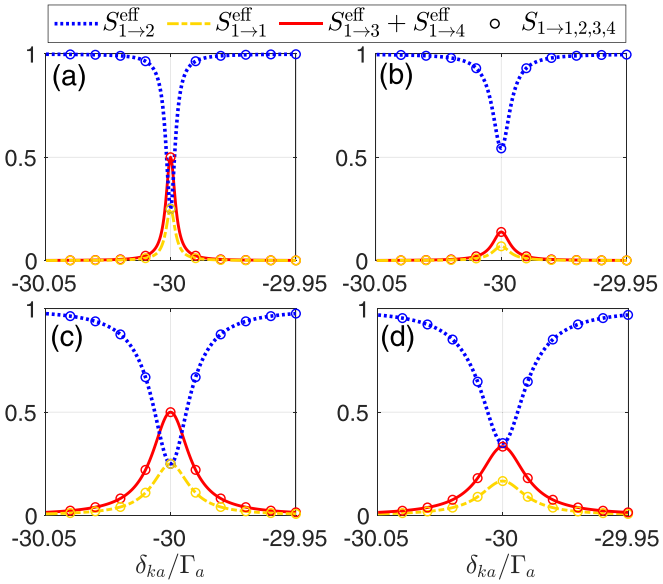

FIG. 5. Effective reflectivity $S^{\rm eff}_{1\to1}$, transmissivity $S^{\rm eff}_{1\to2}$, and total conversion efficiency $S^{\rm eff}_{1\to3}+S^{\rm eff}_{1\to4}$ (compared with $S_{1\to1}$, $S_{1\to2}$, and $S_{1\to3}+S_{1\to4}$) vs detuning δ_{ka} with (a) $\gamma=0$ and $\Omega_{c1}=\Omega_{c2}=\Gamma_a$, (b) $\gamma=10^{-3}\Gamma_a$ and $\Omega_{c1}=\Omega_{c2}=\Gamma_a$, (c) $\gamma=0$ and $\Omega_{c1}=\Omega_{c2}=2\Gamma_a$, and (d) $\gamma=10^{-3}\Gamma_a$ and $\Omega_{c1}=\Omega_{c2}=2\Gamma_a$. Other parameters are $\Delta_{c1}=-\Delta_{c2}=30\Gamma_a$, $V_6=2\times10^4\Gamma_a$, and $\Gamma_a=\Gamma_b=1$ MHz.

Appendix B)

$$S^{\rm eff}_{1\to1}=\left|\frac{-i\Upsilon_a}{i(\Upsilon_a+\Upsilon_b)+(\delta_{ka}+\Delta_{c1}+2i\gamma)}\right|^2,$$
$$S^{\rm eff}_{1\to2}=\left|\frac{i\Upsilon_b+(\delta_{ka}+\Delta_{c1}+2i\gamma)}{i(\Upsilon_a+\Upsilon_b)+(\delta_{ka}+\Delta_{c1}+2i\gamma)}\right|^2,$$
$$S^{\rm eff}_{1\to3}=\left|\frac{-i\sqrt{\Upsilon_a\Upsilon_b}}{i(\Upsilon_a+\Upsilon_b)+(\delta_{ka}+\Delta_{c1}+2i\gamma)}\right|^2,$$
$$S^{\rm eff}_{1\to4}=\left|\frac{-i\sqrt{\Upsilon_a\Upsilon_b}}{i(\Upsilon_a+\Upsilon_b)+(\delta_{ka}+\Delta_{c1}+2i\gamma)}\right|^2, \quad (14)$$

with $\Upsilon_b=\xi_b^2/v_g=\Gamma_b\Omega_{c2}^2/\Delta_{c2}^2$ and $\phi_b=k_bd$. We have also set $\delta_{kb}=\omega_{kb}-\omega_e=-\delta_{ka}$ due to the requirement of energy conservation in a close-loop giant-atom transition with $\Delta_{c2}=-\Delta_{c1}$. Here, $S^{\rm eff}_{1\to1}$ ($S^{\rm eff}_{1\to2}$) denotes the effective reflectivity (transmissivity) of mode a, while $S^{\rm eff}_{1\to3}$ ($S^{\rm eff}_{1\to4}$) refers to the effective backward (forward) conversion efficiencies into waveguide mode b. It is clear that they are *immune* to phases θ_2 and ϕ_b appearing in H_{B_k} since there is only one path for scattering a photon in mode a and converting it into mode b, as shown in Fig. 4(c), where *two-path interference effects* do not occur anymore. Note also that the right-incident case (from port 2) is a symmetric process compared with the left-incident one (from port 1) as considered above because $S^{\rm eff}_{1\to1,2,3,4}$ are reciprocal, being insensitive to relevant phases even if the two driving fields are oblique ($\alpha\neq0$ and $\beta\neq0$).

We plot in Fig. 5 $S^{\rm eff}_{1\to1}$, $S^{\rm eff}_{1\to2}$, and $S^{\rm eff}_{1\to3}+S^{\rm eff}_{1\to4}$ by comparing them with $S_{1\to1}$, $S_{1\to2}$, and $S_{1\to3}+S_{1\to4}$ obtained from the original Hamiltonian H_{B_x} with $\Delta_{c1}=-\Delta_{c2}=30\Gamma_a$. It is evident that the adiabatic elimination of two single-excitation

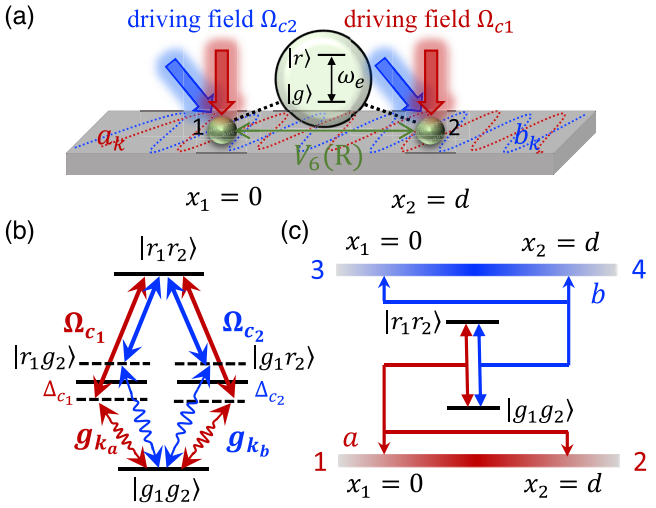

FIG. 6. Schematic diagram for achieving asymmetric frequency conversion between two waveguide modes. (a) The same waveguide-coupled Rydberg-atom platform as in Fig. 4(a) except atoms 1 and 2 are both driven by coherent fields Ω_{c1} and Ω_{c2} at different angles of incidence. (b) The four-level configuration in the two-atom basis where driving field Ω_{c1} (Ω_{c2}) is matched in frequency with waveguide mode a (b) on both left and right paths of two-photon resonance. (c) The equivalent two-level giant atom coupled to each waveguide mode at two points when eliminating two single-excitation states.

states is valid again since there is no difference between $S^{\rm eff}_{1\to j}$ and $S_{1\to j}$. Moreover, the optimal value of frequency conversion efficiency quantified by $S^{\rm eff}_{1\to3}+S^{\rm eff}_{1\to4}$ is only 0.5 when ignoring the intrinsic atomic dissipation ($\gamma=0$) and taking $\Upsilon_a=\Upsilon_b$, as shown in Figs. 5(a) and 5(c). In fact, we have (i) $S^{\rm eff}_{1\to3}\equiv S^{\rm eff}_{1\to4}$ and they are further equal to $S^{\rm eff}_{1\to2}$ if we set $\Upsilon_a=\Upsilon_b$ and (ii) $\sum_{j=1}^4 S^{\rm eff}_{1\to j}\equiv1$ by virtue of energy conservation in the waveguide modes if we set $\gamma=0$, as can be seen from Eq. (14). The inclusion of γ in Figs. 5(b) and 5(d) would lower the conversion efficiency, yet one could increase Rabi frequencies Ω_{c1} and Ω_{c2} to raise $\Upsilon_a=\Upsilon_b$, thus reducing the negative effect of γ. In addition, the sum of $\sum_{j=1}^4 S^{\rm eff}_{1\to j}$ will become less than unity given that a part of energy must leak into the free space from the excited giant atom, though it may approach unity in the far-detuned region. The above findings ($S^{\rm eff}_{1\to3}+S^{\rm eff}_{1\to4}\leqslant0.5$ and $S^{\rm eff}_{1\to3}\equiv S^{\rm eff}_{1\to4}$) prompt us to investigate another scenario for improving the conversion efficiency and meanwhile achieving the asymmetric scattering.

IV. ASYMMETRIC FREQUENCY CONVERSION

We further consider the case where each Rydberg atom is driven by two coherent fields Ω_{c1} and Ω_{c2} as shown in Fig. 6(a). This then results in the four-level configuration in the two-atom basis as shown in Fig. 6(b), where both left and right paths of the two photon resonant transition from ground state $|g_1g_2\rangle$ to double-excitation state $|r_1r_2\rangle$ can be implemented with driving field Ω_{c1} and waveguide mode a or with driving field Ω_{c2} and waveguide mode b. As discussed below, this means of all-optical control will enable one to enhance the efficiency and select the directionality of frequency conversion via tunable chiral couplings, yet without altering

the system's physical structure. The relevant Hamiltonian reads as

$$H_{C_k} = (\omega_e - i\gamma)(|g_1r_2\rangle\langle g_1r_2| + |r_1g_2\rangle\langle r_1g_2|) + (2\omega_e + V_6 - 2i\gamma)|r_1r_2\rangle\langle r_1r_2| + \int dk_a\omega_{ka}a_k^\dagger a_k + \int dk_b\omega_{kb}b_k^\dagger b_k$$
$$+ \Bigg[\int dk_a g_a a_k(|r_1g_2\rangle\langle g_1g_2| + |g_1r_2\rangle\langle g_1g_2|e^{ik_a d}) + \int dk_b g_b b_k(|r_1g_2\rangle\langle g_1g_2| + |g_1r_2\rangle\langle g_1g_2|e^{ik_b d}) + \Omega_{c1}e^{-i\omega_{c1}t}(|r_1r_2\rangle\langle r_1g_2|$$
$$+ e^{i\theta_1}|r_1r_2\rangle\langle g_1r_2|) + \Omega_{c2}e^{-i\omega_{c2}t}(|r_1r_2\rangle\langle r_1g_2| + e^{i\theta_2}|r_1r_2\rangle\langle g_1r_2|) + \text{H.c.}\Bigg], \tag{15}$$

where the two local phase differences θ_1 and θ_2 as defined before can be independently controlled by changing the respective driving fields' angles of incidence.

After adiabatically eliminating the single-excitation states $|r_1g_2\rangle$ and $|g_1r_2\rangle$ in a way similar to that considered in the last two sections, one can attain from H_{C_k} the effective Hamiltonian $H_{C_k}^{\text{eff}}$ (see Appendix C), which if transferred into the real space becomes

$$H_{C_x}^{\text{eff}} = \left(2\omega_e + V_6 - \frac{2\Omega_{c1}^2}{\Delta_{c1}} - \frac{2\Omega_{c2}^2}{\Delta_{c2}} - 2i\gamma\right)|r_1r_2\rangle\langle r_1r_2| + \int_{-\infty}^{+\infty} dx\Bigg[a_L'^\dagger(x)\left(\omega_{c1} + \omega_0 + iv_g\frac{\partial}{\partial x}\right)a_L'(x)$$
$$+ a_R'^\dagger(x)\left(\omega_{c1} + \omega_0 - iv_g\frac{\partial}{\partial x}\right)a_R'(x)\Bigg] + \int_{-\infty}^{+\infty} dx\Bigg[b_L'^\dagger(x)\left(\omega_{c2} + \omega_0 + iv_g\frac{\partial}{\partial x}\right)b_L'(x)$$
$$+ b_R'^\dagger(x)\left(\omega_{c2} + \omega_0 - iv_g\frac{\partial}{\partial x}\right)b_R'(x)\Bigg] + \Bigg\{\int_{-\infty}^{+\infty} dx\xi_a[a_R(x) + a_L(x)]|r_1r_2\rangle\langle g_1g_2|$$
$$\times [\delta(x) + \delta(x-d)e^{i\theta_1}] + \text{H.c.}\Bigg\} + \Bigg\{\int_{-\infty}^{+\infty} dx\xi_b[b_R(x) + b_L(x)]|r_1r_2\rangle\langle g_1g_2|[\delta(x) + \delta(x-d)e^{i\theta_2}] + \text{H.c.}\Bigg\}. \tag{16}$$

Here, the high-frequency oscillation terms $e^{\pm i(\Delta_{c1}+\delta_{kb})t}$ and $e^{\pm i(\Delta_{c2}+\delta_{ka})t}$ have been neglected by assuming $|\Delta_{c1} + \delta_{kb}| \gg g_b\Omega_{c1}/\delta_{kb}$ and $|\Delta_{c2} + \delta_{ka}| \gg g_a\Omega_{c2}/\delta_{ka}$, while taking $\Delta_{c1} + \delta_{ka} \simeq 0$ and $\Delta_{c2} + \delta_{kb} \simeq 0$. This regime corresponds to the case in which detunings Δ_{c1} and Δ_{c2} of the two driving fields are sufficiently large in magnitude and opposite to each other. In this way, as shown in Fig. 6(c), the equivalent two-level system as a combination of the model in Fig. 1(c) and the model in Fig. 4(c) behaves like a giant atom again because it is coupled to both waveguide modes at two points, allowing for the occurrence of self-interference effect for each waveguide mode.

With $H_{C_x}^{\text{eff}}$ in Eq. (16) and taking $|\tilde{\Psi}_{C_x}\rangle = |\tilde{\Psi}_{B_x}\rangle$ in Eq. (13) as the corresponding eigenstate, for a single photon of waveguide mode a incident from port 1 on the left, it is viable to compute (see Appendix C)

$$P_{1\to1}^{\text{eff}} = \left|p_{1\to1}^{\text{eff}}\right|^2 = \left|\frac{-i\Upsilon_a(1 + e^{i\phi_a}e^{i\theta_1})(1 + e^{i\phi_a}e^{-i\theta_1})}{\delta_{ka} + \Delta_{c1} + 2i\gamma + 2i\Upsilon_a(1 + e^{i\phi_a}\cos\theta_1) + 2i\Upsilon_b(1 + e^{i\phi_b}\cos\theta_2)}\right|^2,$$
$$P_{1\to2}^{\text{eff}} = \left|p_{1\to2}^{\text{eff}}\right|^2 = \left|\frac{\delta_{ka} + \Delta_{c1} + 2i\gamma - 2\Upsilon_a e^{i\theta_1}\sin\phi_a + 2i\Upsilon_b(1 + e^{i\phi_b}\cos\theta_2)}{\delta_{ka} + \Delta_{c1} + 2i\gamma + 2i\Upsilon_a(1 + e^{i\phi_a}\cos\theta_1) + 2i\Upsilon_b(1 + e^{i\phi_b}\cos\theta_2)}\right|^2,$$
$$P_{1\to3}^{\text{eff}} = \left|p_{1\to3}^{\text{eff}}\right|^2 = \left|\frac{-i\sqrt{\Upsilon_a\Upsilon_b}(1 + e^{i\phi_b}e^{i\theta_2})(1 + e^{i\phi_a}e^{-i\theta_1})}{\delta_{ka} + \Delta_{c1} + 2i\gamma + 2i\Upsilon_a(1 + e^{i\phi_a}\cos\theta_1) + 2i\Upsilon_b(1 + e^{i\phi_b}\cos\theta_2)}\right|^2,$$
$$P_{1\to4}^{\text{eff}} = \left|p_{1\to4}^{\text{eff}}\right|^2 = \left|\frac{-i\sqrt{\Upsilon_a\Upsilon_b}(1 + e^{-i\phi_b}e^{i\theta_2})(1 + e^{i\phi_a}e^{-i\theta_1})}{\delta_{ka} + \Delta_{c1} + 2i\gamma + 2i\Upsilon_a(1 + e^{i\phi_a}\cos\theta_1) + 2i\Upsilon_b(1 + e^{i\phi_b}\cos\theta_2)}\right|^2, \tag{17}$$

representing, in order, the effective reflectivity, transmissivity, and backward and forward conversion efficiencies. In these expressions, phase difference θ_1 (θ_2) between two driving points of the coherent field Ω_{c1} (Ω_{c2}) will bring about chiral coupling effects together with phase difference ϕ_a (ϕ_b) between two coupling points of the waveguide mode a (b). Then, the scattered photon can be routed toward a selected port while suppressing the probabilities toward other ports, which definitely improves reflectivity $P_{1\to1}^{\text{eff}}$, transmissivity $P_{1\to2}^{\text{eff}}$, or frequency conversion efficiencies $P_{1\to3}^{\text{eff}}$ and $P_{1\to4}^{\text{eff}}$ on demand.

Figure 7 shows typical spectra of the effective reflectivity, transmissivity, and backward and forward conversion efficiencies for different values of relevant phase differences and intrinsic decay rates. It can be seen from Figs. 7(a) and 7(b) that, when the two coherent fields are at normal incidence (i.e., $\theta_1 = \theta_2 = 0$), the equivalent couplings are nonchiral and the optimal frequency conversion efficiency $P_{1\to3}^{\text{eff}} + P_{1\to4}^{\text{eff}} = 0.5$ is the same as that found in the last section. For the perfectly chiral case corresponding to $\theta_1 = \theta_2 = (2n + 1/2)\pi$ and $\phi_a = \phi_b = (2n + 1/2)\pi$ shown in Figs. 7(c) and 7(d), the forward conversion efficiency can approach unity around $\delta_{ka} \simeq -\Delta_{c1}$ with $\gamma = 0$, though in general being smaller than unity for $\gamma \neq 0$. This is because both reflectivity $P_{1\to1}^{\text{eff}}$ and backward conversion efficiency

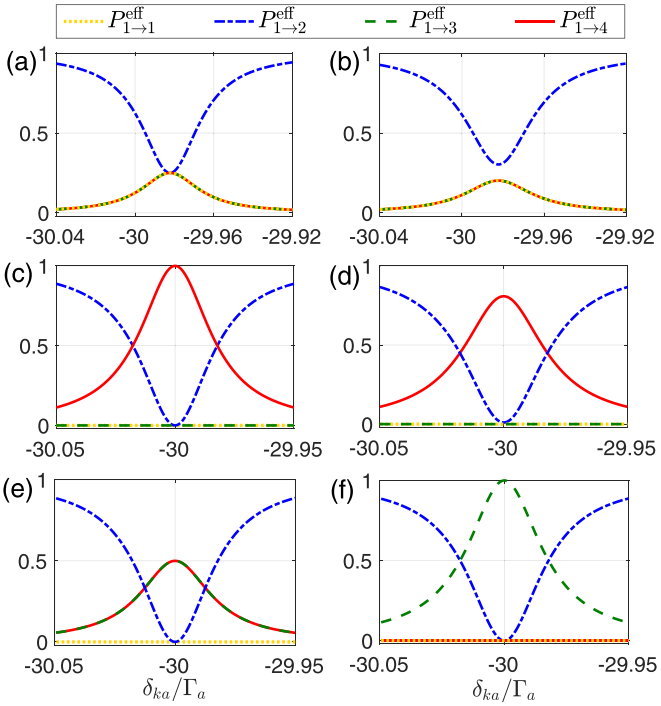

FIG. 7. Effective reflectivity $P^{\rm eff}_{1\to1}$, transmissivity $P^{\rm eff}_{1\to2}$, and backward $P^{\rm eff}_{1\to3}$ and forward $P^{\rm eff}_{1\to4}$ conversion efficiencies vs detuning δ_{ka}. (a), (b) $\phi_b = (2n+1/2)\pi$, $\theta_1 = \theta_2 = 2n\pi$, and $\gamma = 0$ (a) and $\gamma = 10^{-3}\Gamma_a$ (b). (c), (d) $\phi_b = (2n+1/2)\pi, \theta_1 = \theta_2 = (2n+1/2)\pi$, and $\gamma = 0$ (c) and $\gamma = 10^{-3}\Gamma_a$ (d). (e), (f) $\gamma = 0$, $\theta_1 = \theta_2 = (2n+1/2)\pi$, and $\phi_b = (2n+1)\pi$ (e) and $\phi_b = (2n-1/2)\pi$ (f). Other parameters are $\phi_a = (2n+1/2)\pi$, $\Omega_{c1} = \Omega_{c2} = 2\Gamma_a$, $\Delta_{c1} = -\Delta_{c2} = 30\Gamma_a$, $V_6 = 2\times10^4\Gamma_a$, and $\Gamma_a = \Gamma_b = 1$ MHz.

$P^{\rm eff}_{1\to3} = 0$ remain zero, independent of δ_{ka}, as a result of perfect destructive interference contributed by $1 + e^{i\phi_a}e^{i\theta_1}$ and $1 + e^{i\phi_b}e^{i\theta_2}$, respectively, as can be seen from Eq. (17). Hence, our waveguide-coupled Rydberg-atom system is an excellent platform to realize high-efficiency frequency conversion, needing neither multiple-level atomic configurations nor specific devices like Sagnac interferometers [46]. It is also important that one can adjust the output ports of mode b converted from mode a by tuning ϕ_b to attain $P^{\rm eff}_{1\to3} = P^{\rm eff}_{1\to4} = 0.5$ with $\phi_b = (2n+1)\pi$ shown in Fig. 7(e), or $P^{\rm eff}_{1\to3} = 1$ with $\phi_b = (2n-1/2)\pi$ shown in Fig. 7(f), in the ideal case with $\gamma = 0$. As a corollary of this observation, the equivalent chirality of waveguide modes a and b can be controlled separately with different values of ϕ_a and ϕ_b. Indeed, the functions of ϕ_a and θ_1 (ϕ_b and θ_2) are similar, both of which can be used to tune the chirality of waveguide mode a (b) as depicted in Fig. 3(d) only for waveguide mode a.

Based on this chiral coupling mechanism, it is natural to consider the possible realization of asymmetric frequency conversion by comparing scattering behaviors of a left-incident photon with that of a right-incident photon in the same waveguide mode. In fact, for a photon incident from port 2 in mode a, the analytical expression of total conversion efficiency $P^{\rm eff}_{2\to3} + P^{\rm eff}_{2\to4}$ will be identical to that of $P^{\rm eff}_{1\to3} + P^{\rm eff}_{1\to4}$ if we make the replacement $\theta_{1,2} \to -\theta_{1,2}$. It can be found from Figs. 8(a) and 8(b), with $\phi_a = \phi_b = (2n+1/2)\pi$ and $\theta_2 = 0$, that the spectra of the above two conversion efficiencies into

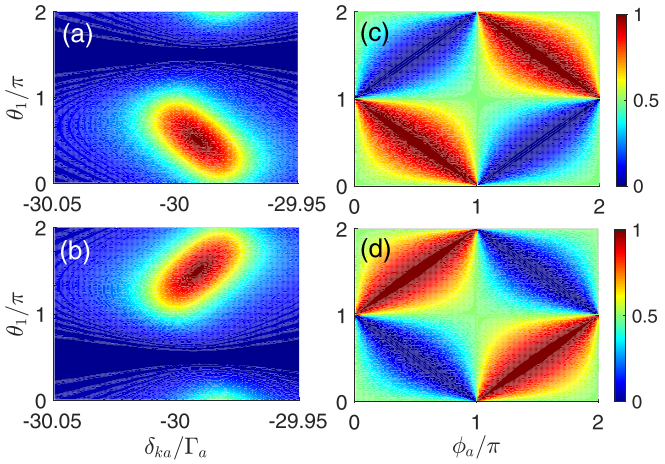

FIG. 8. Effective total conversion efficiency (a), (c) $P^{\rm eff}_{1\to3} + P^{\rm eff}_{1\to4}$ and (b), (d) $P^{\rm eff}_{2\to3} + P^{\rm eff}_{2\to4}$ vs detuning δ_{ka} and phase θ_1 (modulo 2π) with $\phi_a = \phi_b = (2n+1/2)\pi$ (a), (b); vs phases $\phi_b = \phi_a$ (modulo 2π) and θ_1 (modulo 2π) with $\delta_{ka} = -30\Gamma_a$ (c), (d). Other parameters are the same as in Fig. 7 except $\theta_2 = 2n\pi$ and $\gamma = 0$.

mode b have an inverse dependence on θ_1 for the left-incident and right-incident photons in mode a. That means the chirality of mode a is enough to realize asymmetric frequency conversion since it can fully determine whether a photon in mode a can be first absorbed by the two atoms and then converted into mode b while the chirality of mode b will only determine the output port (3 or 4) of the photon converted into mode b. Note also that $P^{\rm eff}_{2\to3} = P^{\rm eff}_{2\to4}$ always holds in Figs. 8(a) and 8(b) due to the fact that $\theta_2 = 0$ refers to the nonchiral case. Figures 8(c) and 8(d) show that ϕ_a and ϕ_b will also determine the chirality, and with $\phi_a = \phi_b = n\pi$ the frequency conversion turns out to be symmetric, which is consistent with Fig. 3(d).

V. CONCLUSIONS

Waveguide-coupled Rydberg atoms represent a relatively new form of hybrid quantum systems, made of individual components with complementary characteristics, e.g., long coherence times, flexible all-optical control, and available transition frequencies; these systems are of interest to a wide range of areas, from quantum computation and communication to quantum sensing. The present paper represents a detailed and systematic account of the large degree of control over the range and the nature of equivalent chiral couplings and nonreciprocal scattering enabled by two Rydberg atoms coupled to a waveguide so as to form a giant atom. Our waveguide-coupled Rydberg giant-atom platform may also be adapted to work as a frequency converter with an efficiency that can exhibit a strong asymmetry and be significantly enhanced via chiral couplings. It is certainly noteworthy to mention here that our model can be easily expanded to accomplish a multifrequency conversion. This entails incorporating additional driving fields with varying frequencies, coupled to the upper transitions, to successfully implement two-photon transitions. We believe that our proposal provides an innovative approach to chiral giant-atom physics and one that may lead to novel results on the Rydberg nonlinearity at optical frequencies.

ACKNOWLEDGMENTS

This work is supported by the National Natural Science Foundation of China (Grants No. 12074061, No. 62375047, and No. 12375010), Jilin Province of China (Grant No. 20220502002GH), the Italian PNRR MUR (Grant No. PE0000023-NQSTI), European Union, Next Generation EU' Integrated Infrastructure Initiative in Photonic and Quantum Sciences (I-PHOQS, IR0000016, ID D2B8D520), and the Fund for International Activities at the University of Brescia. Y.T.C. and J.H.W. would like to thank Scuola Normale Superiore for the hospitality.

APPENDIX A: NONRECIPROCAL TRANSMISSION WITH ONE SINGLE FIELD

1. Two Rydberg atoms without any constraints

Here we would like to show how to apply the Bethe-ansatz approach to solve the scattering problem for the two Rydberg atoms. By solving the eigenequation $H_{A_x}|\Psi_{A_x}\rangle = \omega_{ka}|\Psi_{A_x}\rangle$ from Eqs. (2) and (3) in the main text, one can obtain

$$\begin{aligned}
\omega_{ka}\Phi^A_{aR}(x) &= e^{ik_0x}\left(\omega_0 - iv_g\frac{\partial}{\partial x}\right)\Phi^A_{aR}(x)e^{-ik_0x} + g_a\delta(x)u^A_b + g_a\delta(x-d)u^A_c,\\
\omega_{ka}\Phi^A_{aL}(x) &= e^{-ik_0x}\left(\omega_0 + iv_g\frac{\partial}{\partial x}\right)\Phi^A_{aL}(x)e^{ik_0x} + g_a\delta(x)u^A_b + g_a\delta(x-d)u^A_c,\\
\omega_{ka}u^A_b &= (\omega_e - i\gamma)u^A_b + g_a\left[\Phi^A_R(0) + \Phi^A_L(0)\right] + \Omega_{c1}u^A_d,\\
\omega_{ka}u^A_c &= (\omega_e - i\gamma)u^A_c + g_a\left[\Phi^A_R(d) + \Phi^A_L(d)\right] + \Omega_{c1}e^{-i\theta_1}u^A_d,\\
\omega_{ka}u^A_d &= (\omega_e - \Delta_{c1} - 2i\gamma)u^A_d + \Omega_{c1}u^A_b + \Omega_{c1}e^{i\theta_1}u^A_c,
\end{aligned} \tag{A1}$$

where ω_{ka} is the frequency of one incident photon satisfying $\omega_{ka} = \omega_0 + (k_a - k_0)v_g$. For the left-incident case (from port 1), substituting the wave functions $\Phi^A_{aR,aL}(x)$ in Eq. (4) into Eq. (A1), we obtain

$$\begin{aligned}
0 &= -iv_g(A_1 - 1) + g_a u^A_b,\\
0 &= -iv_g(t_{1\to2} - A_1)e^{i\phi_a} + g_a u^A_c,\\
0 &= -iv_g(r_{1\to1} - A_2) + g_a u^A_b,\\
0 &= -iv_g A_2 e^{-i\phi_a} + g_a u^A_c,\\
0 &= \frac{g_a}{2}(A_1 + A_2 + r_{1\to1} + 1) + \Omega_{c1}u^A_d - (\delta_{ka} + i\gamma)u^A_b,\\
0 &= \frac{g_a}{2}(A_1e^{i\phi_a} + A_2e^{-i\phi_a} + t_{1\to2}e^{i\phi_a}) + \Omega_{c1}e^{-i\theta_1}u^A_d - (\delta_{ka} + i\gamma)u^A_c,\\
0 &= \Omega_{c1}u^A_b + \Omega_{c1}e^{i\theta_1}u^A_c - (\delta_{ka} + \Delta_{c1} + 2i\gamma)u^A_d
\end{aligned} \tag{A2}$$

with $\phi_a = k_a d = k_0 d + (\omega_{ka} - \omega_0)d/v_g$ that can be seen as a constant in the Markovian regime [39] and $\delta_{ka} = \omega_{ka} - \omega_e$. Then solving Eq. (A2) numerically, one can get the transmissivity from port 1 to port 2 as $T_{1\to2} = |t_{1\to2}|^2$. If the photon is incident from the right port, i.e., port 2, then one can similarly substitute Eq. (5) into Eq. (A1) to obtain the transmissivity from port 2 to port 1. It can be found that all the results are the same compared with the left-incident case yet with an opposite sign of the phase difference, i.e., $\theta_1 \leftrightarrow -\theta_1$.

2. Equivalent giant atom with large detunings

Based on the effective Hamiltonian theory [56,57], for the model shown in Fig. 1 in the main text, we first need to obtain the Hamiltonian in the interaction picture from H_{A_k} in Eq. (1) as

$$\begin{aligned}
\mathcal{H}_{A_k}(t) &= i\frac{dU_1^\dagger}{dt}U_1 + U_1^\dagger H_{A_k}U_1\\
&= \int dk_a g_a a_{ka}(|r_1g_2\rangle\langle g_1g_2| + |g_1r_2\rangle\langle g_1g_2|e^{ik_ad})e^{-i\delta_{ka}t} + \Omega_{c1}e^{-i\Delta_{c1}t}(|r_1r_2\rangle\langle r_1g_2| + e^{i\theta_1}|r_1r_2\rangle\langle g_1r_2|) + \text{H.c.},
\end{aligned} \tag{A3}$$

where the unitary operator $U_1 = e^{-iH_{A_1}t}$ with $H_{A_1} = \omega_e(|g_1r_2\rangle\langle g_1r_2| + |r_1g_2\rangle\langle r_1g_2|) + (2\omega_e + V_6)|r_1r_2\rangle\langle r_1r_2| + \int dk_a\omega_{ka}a_{ka}^\dagger a_{ka}$. Then the effective Hamiltonian in the interaction picture can be obtained as

$$\begin{aligned}\mathcal{H}_{A_k}^{\rm eff}(t) &= -i\mathcal{H}_{A_k}(t)\int_0^t \mathcal{H}_{A_k}(t')dt' \\ &\simeq \frac{2g_a^2}{\delta_{ka}}\int dk_a a_{ka}a_{ka}^\dagger|g_1g_2\rangle\langle g_1g_2| - \frac{2\Omega_{c1}^2}{\Delta_{c1}}|r_1r_2\rangle\langle r_1r_2| - 2i\gamma|r_1r_2\rangle\langle r_1r_2| \\ &\quad + \frac{g_a\Omega_{c1}e^{i\theta_1}}{\delta_{ka}}\int dk_a a_{ka}e^{-i(\delta_{ka}+\Delta_{c1})t}|r_1r_2\rangle\langle g_1g_2|(1+e^{ik_ad}) \\ &\quad - \frac{g\Omega_{c1}e^{-i\theta_1}}{\Delta_{c1}}\int dk_a a_{ka}^\dagger e^{i(\delta_{ka}+\Delta_{c1})t}|g_1g_2\rangle\langle r_1r_2|(1+e^{-ik_ad}) + \cdots, \end{aligned} \tag{A4}$$

where we have omitted a few terms related to the single-excitation states $|r_1g_2\rangle$ and $|g_1r_2\rangle$ since they are decoupled from other states and only interact with each other. Assuming $\Delta_{c1} + \delta_{ka} \simeq 0$ and $|\Delta_{c1}|, |\delta_{ka}| \gg \Omega_{c1}, g_a$, we will have the effective Hamiltonian in the Schrödinger picture as

$$\begin{aligned}H_{A_k}^{\rm eff} &= i\frac{dU_2^\dagger}{dt}U_2 + U_2^\dagger\mathcal{H}_{A_k}^{\rm eff}(t)U_2 \\ &= \left(2\omega_e + V_6 - \frac{2\Omega_{c1}^2}{\Delta_{c1}} - 2i\gamma\right)|r_1r_2\rangle\langle r_1r_2| + \int dk_a(\omega_{ka}+\omega_{c1})a_{ka}^\dagger a_{ka} + \int dk_a\xi_a a_{ka}(1+e^{ik_ad}e^{i\theta_1})|r_1r_2\rangle\langle g_1g_2| + \text{H.c.},\end{aligned} \tag{A5}$$

where $\xi_a = -g_a\Omega_{c1}/\Delta_{c1}$ and $U_2 = e^{-iH_{A_2}t}$ with $H_{A_2} = -(2\omega_e + V_6)|r_1r_2\rangle\langle r_1r_2| - \int dk_a(\omega_{ka}+\omega_{c1})a_{ka}^\dagger a_{ka}$. Then this effective momentum-space Hamiltonian can be transformed to the real space as in Eq. (6) in the main text.

Then, with the same procedure, by solving the eigenequation $H_{A_x}^{\rm eff}|\tilde\Psi_{A_x}\rangle = (\omega_{ka}+\omega_{c1})|\tilde\Psi_{A_x}\rangle$ from Eqs. (6) and (7) in the main text, one can get the following equations:

$$\begin{aligned}(\omega_{ka}+\omega_{c1})\tilde\Phi_{aR}^A(x) &= e^{ik_0x}\left(\omega_{c1}+\omega_0 - iv_g\frac{\partial}{\partial x}\right)\tilde\Phi_{aR}^A(x)e^{-ik_0x} + \xi_a[\delta(x) + e^{i\theta_1}\delta(x-d)]\tilde u_d^A, \\ (\omega_{ka}+\omega_{c1})\tilde\Phi_{aL}^A(x) &= e^{-ik_0x}\left(\omega_{c1}+\omega_0 + iv_g\frac{\partial}{\partial x}\right)\tilde\Phi_{aL}^A(x)e^{ik_0x} + \xi_a[\delta(x) + e^{i\theta_1}\delta(x-d)]\tilde u_d^A, \\ (\omega_{ka}+\omega_{c1})\tilde u_d^A &= \left(2\omega_e + V_6 - \frac{2\Omega_{c1}^2}{\Delta_{c1}} - 2i\gamma\right)\tilde u_d^A + \xi_a\left[\tilde\Phi_{aR}^A(0) + \tilde\Phi_{aL}^A(0)\right] + \xi_a e^{-i\theta_1}\left[\tilde\Phi_{aR}^A(d) + \tilde\Phi_{aL}^A(d)\right]\end{aligned} \tag{A6}$$

and

$$\begin{aligned}0 &= -iv_g\left(A_1^{\rm eff} - 1\right) + \xi_a\tilde u_d^A, \\ 0 &= -iv_g\left(t_{1\to2}^{\rm eff} - A_1^{\rm eff}\right)e^{i\phi_a} + \xi_a e^{i\theta_1}\tilde u_d^A, \\ 0 &= -iv_g\left(r_{1\to1}^{\rm eff} - A_2^{\rm eff}\right) + \xi_a\tilde u_d^A, \\ 0 &= -iv_gA_2^{\rm eff}e^{-i\phi_a} + \xi_a e^{i\theta_1}\tilde u_d^A, \\ 0 &= \frac{\xi_a}{2}\left(A_1^{\rm eff} + A_2^{\rm eff} + r_{1\to1}^{\rm eff} + 1\right) + \frac{\xi_a}{2}e^{-i\theta_1}\left(A_1^{\rm eff}e^{i\phi_a} + A_2^{\rm eff}e^{-i\phi_a} + t_{1\to2}^{\rm eff}e^{i\phi_a}\right) - \left(\delta_{ka} + \Delta_{c1} + \frac{2\Omega_{c1}^2}{\Delta_{c1}} + 2i\gamma\right)\tilde u_d^A.\end{aligned} \tag{A7}$$

The effective transmissivity $T_{1\to2}^{\rm eff} = |t_{1\to2}^{\rm eff}|^2$ of Eq. (8) can be obtained from solving Eq. (A7). The transmissivity $T_{2\to1}^{\rm eff} = |t_{2\to1}^{\rm eff}|^2$ in Eq. (8) of a right-incident photon is dealt with in the same way as above.

3. Continuous-coupling case based on dynamical solution method

In the case of continuous coupling, elucidating the wave-function ansatz in real space can be challenging, particularly due to the unclear delineation of the coupling region. Therefore, we are considering the application of the dynamical solution method based on the momentum-space description [28,54]. Additionally, we illustrate the process of obtaining transmissivities for the pointlike coupling case once again, providing an example. Based on the effective Hamiltonian in Eq. (A5), the time-evolving state at time t in the single-excitation invariant subspace can be written as

$$\left|\Psi_{A_k}(t)\right\rangle = \int dk_a[c_1(t)a_{kR}^\dagger + c_2(t)a_{kL}^\dagger]|0, g_1g_2\rangle + \tilde u_d^A(t)|0, r_1r_2\rangle. \tag{A8}$$

Therefore, we have the dynamical equations for the equivalent giant atom:

$$\begin{aligned}
\partial_t \tilde{u}_d^A(t) &= -\left(i\omega_e - i\Delta_{c1} - i\frac{2\Omega_{c1}^2}{\Delta_{c1}} + 2\gamma\right)\tilde{u}_d^A(t) - i\xi\int dk_a(1+e^{ik_a d}e^{-i\theta_1})c_1(t) - i\xi\int dk_a(1+e^{-ik_a d}e^{-i\theta_1})c_2(t),\\
\partial_t c_1(t) &= -i\omega_{ka}c_1(t) - i\tilde{u}_d^A(t)\xi(1+e^{-ik_a d}e^{i\theta_1}),\\
\partial_t c_2(t) &= -i\omega_{ka}c_2(t) - i\tilde{u}_d^A(t)\xi(1+e^{ik_a d}e^{i\theta_1})
\end{aligned} \tag{A9}$$

with $\xi = \xi_a/\sqrt{2\pi}$. $c_1(t)$ and $c_2(t)$ refer to the right- and left-propagating fields, respectively. Integrating the latter two equations, we have

$$\begin{aligned}
c_1(t) &= e^{-i\omega_{ka}t}\left[c_1(0) - i\xi(1+e^{-ik_a d}e^{i\theta_1})\int_0^t dt'\tilde{u}_d^A(t')e^{i\omega_{ka}t'}\right],\\
c_2(t) &= e^{-i\omega_{ka}t}\left[c_2(0) - i\xi(1+e^{ik_a d}e^{i\theta_1})\int_0^t dt'\tilde{u}_d^A(t')e^{i\omega_{ka}t'}\right].
\end{aligned} \tag{A10}$$

Inserting these two equations into the dynamical equation of $\tilde{u}_d^A(t)$ in Eq. (A9) and after arranging, we have

$$\begin{aligned}
\partial_t \tilde{u}_d^A(t) &= -\left(i\omega_e - i\Delta_{c1} - i\frac{2\Omega_{c1}^2}{\Delta_{c1}} + 2\gamma\right)\tilde{u}_d^A(t) - i\frac{\xi}{v_g}\int d\omega_{ka}(1+e^{i\omega_{ka}d/v_g}e^{-i\theta_1})e^{-i\omega_{ka}t}c_1(0)\\
&\quad - i\frac{\xi}{v_g}\int d\omega_{ka}(1+e^{-i\omega_{ka}d/v_g}e^{-i\theta_1})e^{-i\omega_{ka}t}c_2(0)\\
&\quad - \frac{\xi^2}{v_g}\int_0^t dt'\tilde{u}_d^A(t')\int d\omega_{ka}\left[2e^{-i\omega_{ka}(t-t')} + e^{-i\omega_{ka}(t-t'-d/v_g)}e^{-i\theta_1} + e^{-i\omega_{ka}(t-t'+d/v_g)}e^{i\theta_1}\right]\\
&\quad - \frac{\xi^2}{v_g}\int_0^t dt'\tilde{u}_d^A(t')\int d\omega_{ka}\left[2e^{-i\omega_{ka}(t-t')} + e^{-i\omega_{ka}(t-t'-d/v_g)}e^{i\theta_1} + e^{-i\omega_{ka}(t-t'+d/v_g)}e^{-i\theta_1}\right]\\
&= -\left(i\omega_e - i\Delta_{c1} - i\frac{2\Omega_{c1}^2}{\Delta_{c1}} + 2\gamma\right)\tilde{u}_d^A(t) - i\frac{\xi}{v_g}\int d\omega_{ka}(1+e^{i\omega_{ka}d/v_g}e^{-i\theta_1})e^{-i\omega_{ka}t}c_1(0)\\
&\quad - i\frac{\xi}{v_g}\int d\omega_{ka}(1+e^{-i\omega_{ka}d/v_g}e^{-i\theta_1})e^{-i\omega_{ka}t}c_2(0)\\
&\quad - \frac{2\pi\xi^2}{v_g}\int_0^t dt'\tilde{u}_d^A(t')[2\delta(t-t') + \delta(t'-t+d/v_g)e^{-i\theta_1} + \delta(t'-t-d/v_g)e^{i\theta_1}]\\
&\quad - \frac{2\pi\xi^2}{v_g}\int_0^t dt'\tilde{u}_d^A(t')[2\delta(t-t') + \delta(t'-t+d/v_g)e^{i\theta_1} + \delta(t'-t-d/v_g)e^{-i\theta_1}]\\
&= -\left(i\omega_e - i\Delta_{c1} - i\frac{2\Omega_{c1}^2}{\Delta_{c1}} + 2\gamma\right)\tilde{u}_d^A(t) - i\frac{\xi}{v_g}\int d\omega_{ka}(1+e^{i\omega_{ka}d/v_g}e^{-i\theta_1})e^{-i\omega_{ka}t}c_1(0)\\
&\quad - i\frac{\xi}{v_g}\int d\omega_{ka}(1+e^{-i\omega_{ka}d/v_g}e^{-i\theta_1})e^{-i\omega_{ka}t}c_2(0)\\
&\quad - \frac{4\pi\xi^2}{v_g}\tilde{u}_d^A(t) - \frac{2\pi\xi^2}{v_g}\Theta(t-d/v_g)\tilde{u}_d^A(t-d/v_g)e^{-i\theta_1} - \frac{2\pi\xi^2}{v_g}\Theta(t-d/v_g)\tilde{u}_d^A(t-d/v_g)e^{i\theta_1}.
\end{aligned} \tag{A11}$$

Here, we have assumed $\tilde{u}_d^A(t) = 0$ for $t < 0$ and thus neglected the Heaviside step function $\Theta(t-d/v_g)$. By Fourier transforming this equation and with the initial condition $\tilde{u}_d^A(0) = 0$, we have

$$\begin{aligned}
-i\tilde{u}_d^A(\omega_{ka}) &= -\left(i\omega_e - i\Delta_{c1} - i\frac{2\Omega_{c1}^2}{\Delta_{c1}} + 2\gamma\right)\tilde{u}_d^A(\omega_{ka}) - i\frac{2\pi\xi}{v_g}(1+e^{i\omega_{ka}d/v_g}e^{-i\theta_1})c_1(0) - i\frac{2\pi\xi}{v_g}(1+e^{-i\omega_{ka}d/v_g}e^{-i\theta_1})c_2(0)\\
&\quad - \frac{4\pi\xi^2}{v_g}\tilde{u}_d^A(\omega_{ka}) - \frac{4\pi\xi^2}{v_g}\tilde{u}_d^A(\omega_{ka})e^{i\omega_a d/v_g}\cos\theta_1,
\end{aligned} \tag{A12}$$

and

$$\tilde{u}_d^A(t) = \int d\omega_{ka}\frac{\frac{\xi}{v_g}(1+e^{i\omega_{ka}d/v_g}e^{-i\theta_1})c_1(0) + \frac{\xi}{v_g}(1+e^{-i\omega_{ka}d/v_g}e^{-i\theta_1})c_2(0)}{\omega_{ka} - \omega_e + \Delta_{c1} + \frac{2\Omega_{c1}^2}{\Delta_{c1}} + 2i\gamma + i\frac{4\pi\xi^2}{v_g}(1+e^{i\omega_{ka}d/v_g}\cos\theta_1)}e^{-i\omega_{ka}t}. \tag{A13}$$

For the left-incident photon with $c_1(0) \neq 0$ and $c_2(0) = 0$, we substitute this equation into the equation of $c_1(t)$:

$$c_1(t) = e^{-i\omega_{ka}t}c_1(0) - i\frac{\xi^2}{v_g}(1 + e^{-i\omega_{ka}d/v_g}e^{i\theta_1})\int d\omega'_{ka}\frac{(1 + e^{i\omega'_{ka}d/v_g}e^{-i\theta_1})c_1(0)}{\omega'_{ka} - \omega_e + \Delta_{c1} + \frac{2\Omega_{c1}^2}{\Delta_{c1}} + 2i\gamma + i\frac{4\pi g^2}{v_g}(1 + e^{i\omega'_{ka}d/v_g}\cos\theta_1)}$$
$$\times e^{-i\omega_{ka}t}\int_0^t dt'\tilde{u}_d^A(t')e^{i(\omega_{ka}-\omega'_{ka})t'},$$
$$c_1(\infty) = e^{-i\omega_{ka}t}c_1(0)\left(1 - i\frac{4\pi\xi^2}{v_g}\frac{1 + \cos(\omega_{ka}d/v_g)\cos\theta_1 + \sin(\omega_{ka}d/v_g)\sin\theta_1}{\omega_{ka} - \omega_e + \Delta_{c1} + \frac{2\Omega_{c1}^2}{\Delta_{c1}} + 2i\gamma + i\frac{4\pi\xi^2}{v_g}(1 + e^{i\omega_{ka}d/v_g}\cos\theta_1)}\right), \tag{A14}$$

which is in the long-time limit. Therefore, the transmissivity $T_{1\to2}^{\text{eff}} \equiv \frac{|c_1(\infty)|^2}{|c_1(0)|^2}$ can be expressed as

$$T_{1\to2}^{\text{eff}} = \left|\frac{\delta_{ka} + \Delta_{c1} + \frac{2\Omega_{c1}^2}{\Delta_{c1}} + 2i\gamma - 2\Upsilon_a e^{i\theta_1}\sin\phi_a}{\delta_{ka} + \Delta_{c1} + \frac{2\Omega_{c1}^2}{\Delta_{c1}} + 2i\gamma + 2i\Upsilon_a(1 + e^{i\phi_a}\cos\theta_1)}\right|^2 \tag{A15}$$

with $\Upsilon_a = \xi_a^2/v_g$, which is the same as that in Eq. (8) in the main text calculated from the Bethe-ansatz method.

Taking continuous coupling into account, considering the example with the coupling distribution represented by exponential functions as $\nu_1(x) = \frac{\xi}{\Lambda}e^{-\frac{2}{\Theta}|x|}$ at $x = 0$ and $\nu_2(x) = \frac{\xi}{\Lambda}e^{-\frac{2}{\Theta}|x-d|}$ at $x = d$, the momentum-space Hamiltonian can be written as

$$H_{A_k}^{\text{eff}_c} = \left(2\omega_e + V_6 - \frac{2\Omega_{c1}^2}{\Delta_{c1}} - 2i\gamma\right)|r_1r_2\rangle\langle r_1r_2| + \int dk_a(\omega_{ka} + \omega_{c1})(a_{kL}^\dagger a_{kL} + a_{kR}^\dagger a_{kR})$$
$$+ \int dx\int dk_a\{a_{kL}^\dagger|g\rangle\langle e|[\nu_1(x) + \nu_2(x)]e^{ik_ax}e^{i\theta(x)} + a_{kR}^\dagger|g\rangle\langle e|[\nu_1(x) + \nu_2(x)]e^{-ik_ax}e^{i\theta(x)}$$
$$+ a_{kL}|e\rangle\langle g|[\nu_1(x) + \nu_2(x)]e^{-ik_ax}e^{-i\theta(x)} + a_{kR}|e\rangle\langle g|[\nu_1(x) + \nu_2(x)]e^{ik_ax}e^{-i\theta(x)}\}, \tag{A16}$$

where Λ is the characteristic width and $\int dx\nu_{1,2}(x) = \xi$ is satisfied. The coupling phase difference is no longer a constant which should be expressed as a function of position $\theta(x) = x\theta_1/d$ assuming that the driving field is incident with an unchanged angle. Then the dynamical equations become

$$\partial_t\tilde{u}_d^{A_c}(t) = -\left(i\omega_e - i\Delta_{c1} - i\frac{2\Omega_{c1}^2}{\Delta_{c1}} + 2\gamma\right)\tilde{u}_d^{A_c}(t) - i\int dx\int dk_a[\nu_1(x) + \nu_2(x)]e^{ik_ax}e^{-i\theta(x)}z_1(t)$$
$$- i\int dx\int dk_a[\nu_1(x) + \nu_2(x)]e^{-ik_ax}e^{-i\theta(x)}z_2(t),$$
$$\partial_t z_1(t) = -i\omega_{ka}z_1(t) - i\tilde{u}_d^{A_c}(t)\int dx[\nu_1(x) + \nu_2(x)]e^{-ik_ax}e^{i\theta(x)},$$
$$\partial_t z_2(t) = -i\omega_{ka}z_2(t) - i\tilde{u}_d^{A_c}(t)\int dx[\nu_1(x) + \nu_2(x)]e^{ik_ax}e^{i\theta(x)}. \tag{A17}$$

With the same procedure, we have

$$\partial_t\tilde{u}_d^{A_c}(t) = -\left(i\omega_e - i\Delta_{c1} - i\frac{2\Omega_{c1}^2}{\Delta_{c1}} + 2\gamma\right)\tilde{u}_d^{A_c}(t) - \frac{i}{v_g}\int dx\int d\omega_{ka}[\nu_1(x) + \nu_2(x)]e^{i\omega_{ka}x/v_g}e^{-i\theta(x)}e^{-i\omega_{ka}t}z_1(0)$$
$$- \frac{i}{v_g}\int dx\int d\omega_{ka}[\nu_1(x) + \nu_2(x)]e^{-i\omega_{ka}x/v_g}e^{-i\theta(x)}e^{-i\omega_{ka}t}z_2(0)$$
$$- \frac{1}{2v_g}\int_0^t dt'\tilde{u}_d^{A_c}(t')\int dx\int dx'\int d\omega_{ka}[\nu_1(x)\nu_1(x') + \nu_1(x)\nu_2(x') + \nu_1(x')\nu_2(x) + \nu_2(x)\nu_2(x')]$$
$$\times\left[e^{-i\omega_{ka}[t-t'-|x-x'|/v_g]} + e^{-i\omega_{ka}[t-t'+|x-x'|/v_g]}\right]\left(e^{-i\theta|x-x'|} + e^{i\theta|x-x'|}\right)$$
$$= -\left(i\omega_e - i\Delta_{c1} - i\frac{2\Omega_{c1}^2}{\Delta_{c1}} + 2\gamma\right)\tilde{u}_d^{A_c}(t) - \frac{i}{v_g}\int dx\int d\omega_{ka}[\nu_1(x) + \nu_2(x)]e^{i\omega_{ka}x/v_g}e^{-i\theta(x)}e^{-i\omega_{ka}t}z_1(0)$$
$$- \frac{i}{v_g}\int dx\int d\omega_{ka}[\nu_1(x) + \nu_2(x)]e^{-i\omega_{ka}x/v_g}e^{-i\theta(x)}e^{-i\omega_{ka}t}z_2(0)$$
$$- \frac{\pi}{v_g}\int_0^t dt'\tilde{u}_d^{A_c}(t')\int dx\int dx'\int d\omega_{ka}[\nu_1(x)\nu_1(x') + \nu_1(x)\nu_2(x') + \nu_1(x')\nu_2(x) + \nu_2(x)\nu_2(x')]$$
$$\times[\delta(t' - t + |x - x'|/v_g) + \delta(t' - t - |x - x'|/v_g)](e^{-i\theta|x-x'|} + e^{i\theta|x-x'|})$$

$$
\begin{aligned}
&= -\left(i\omega_e - i\Delta_{c1} - i\frac{2\Omega_{c1}^2}{\Delta_{c1}} + 2\gamma\right)\tilde{u}_d^{A_c}(t) - \frac{i}{v_g}\int dx \int d\omega_{ka}[\nu_1(x)+\nu_2(x)]e^{i\omega_{ka}x/v_g}e^{-i\theta(x)}e^{-i\omega_{ka}t}z_1(0) \\
&\quad - \frac{i}{v_g}\int dx \int d\omega_{ka}[\nu_1(x)+\nu_2(x)]e^{-i\omega_{ka}x/v_g}e^{-i\theta(x)}e^{-i\omega_{ka}t}z_2(0) \\
&\quad - \frac{\pi}{v_g}\int_0^t dt'\tilde{u}_d^{A_c}(t')\int dx\int dx'\int d\omega_{ka}[\nu_1(x)\nu_1(x')+\nu_1(x)\nu_2(x')+\nu_1(x')\nu_2(x)+\nu_2(x)\nu_2(x')] \\
&\quad \times [\Theta(t-|x-x'|/v_g)\tilde{u}_d^{A_c}(t-|x-x'|/v_g)](e^{-i\theta|x-x'|}+e^{i\theta|x-x'|}).
\end{aligned} \tag{A18}
$$

After Fourier transforming this equation as

$$
\tilde{u}_d^{A_c}(\omega_{ka}) = \frac{\frac{2\pi}{v_g}\int dx[\nu_1(x)+\nu_2(x)]e^{i\omega_{ka}x/v_g}e^{-i\theta(x)}z_1(0) + \frac{2\pi}{v_g}\int dx[\nu_1(x)+\nu_2(x)]e^{-i\omega_{ka}x/v_g}e^{-i\theta(x)}z_2(0)}{\omega_{ka}-\omega_e+\Delta_{c1}+\frac{2\Omega_{c1}^2}{\Delta_{c1}}+2i\gamma+F} \tag{A19}
$$

with $F = i\frac{2\pi}{v_g}\int dx\int dx'[\nu_1(x)\nu_1(x')+\nu_1(x)\nu_2(x')+\nu_1(x')\nu_2(x)+\nu_2(x)\nu_2(x')]e^{i\omega_{ka}|x-x'|/v_g}(e^{-i\theta|x-x'|}+e^{i\theta|x-x'|})$, we replace $\int dx\nu_{1,2}(x)$ to $\sqrt{\frac{v_g}{2\pi}}\int d\varphi\tilde{\nu}_{1,2}(\varphi)$ with $\tilde{\nu}_1(\varphi) = \frac{\sqrt{\Upsilon_a}}{\Lambda}e^{-\frac{2}{\Lambda}|\varphi|}$, $\tilde{\nu}_2(\varphi) = \frac{\sqrt{\Upsilon_a}}{\Lambda}e^{-\frac{2}{\Upsilon_1}|\varphi-(\omega_{ka}/v_g\pm\theta_1/d)d|}$, and $\varphi = (\omega_{ka}/v_g \pm \theta_1/d)x$. We have

$$
\tilde{u}_d^{A_c}(t) = \int d\omega_{ka}\frac{\frac{1}{\sqrt{2\pi v_g}}\left\{\int d\varphi[\tilde{\nu}_1(\varphi)+\tilde{\nu}_2(\varphi)]e^{i\omega_{ka}x/v_g}e^{-i\theta(x)}z_1(0) + \int d\varphi[\tilde{\nu}_1(\varphi)+\tilde{\nu}_2(\varphi)]e^{-i\omega_{ka}x/v_g}e^{-i\theta(x)}z_2(0)\right\}}{\omega_{ka}-\omega_e+\Delta_{c1}+\frac{2\Omega_{c1}^2}{\Delta_{c1}}+2i\gamma+i(2\Gamma+2iJ+\Gamma_{ex}+\Gamma'_{ex}+iJ_{ex}+iJ'_{ex})}e^{-i\omega_{ka}t}, \tag{A20}
$$

where

$$
\Gamma = \int_{-\infty}^{\infty}d\varphi\int_{-\infty}^{\infty}d\varphi'\tilde{\nu}_1(\varphi)\tilde{\nu}_1(\varphi')\cos(\varphi-\varphi') = \int_{-\infty}^{\infty}d\varphi\int_{-\infty}^{\infty}d\varphi'\tilde{\nu}_2(\varphi)\tilde{\nu}_2(\varphi')\cos(\varphi-\varphi') = \frac{16\Upsilon_a}{(\Lambda^2+4)^2}, \tag{A21}
$$

$$
J = \int_{-\infty}^{\infty}d\varphi\int_{-\infty}^{\infty}d\varphi'\tilde{\nu}_1(\varphi)\tilde{\nu}_1(\varphi')\sin|\varphi-\varphi'| = \int_{-\infty}^{\infty}d\varphi\int_{-\infty}^{\infty}d\varphi'\tilde{\nu}_2(\varphi)\tilde{\nu}_2(\varphi')\sin|\varphi-\varphi'| = \frac{\Upsilon_a\Lambda(\Lambda^2+12)}{(\Lambda^2+4)^2}, \tag{A22}
$$

$$
\Gamma_{ex} = \int_{-\infty}^{\infty}d\varphi\int_{-\infty}^{\infty}d\varphi'\tilde{\nu}_1(\varphi)\tilde{\nu}_2(\varphi')\cos(\varphi-\varphi') = \frac{16\Upsilon_a\cos[(\omega_{ka}/v_g+\theta_1/d)d]}{(\Lambda^2+4)^2}, \quad x>x', \tag{A23}
$$

$$
\Gamma'_{ex} = \int_{-\infty}^{\infty}d\varphi\int_{-\infty}^{\infty}d\varphi'\tilde{\nu}_1(\varphi)\tilde{\nu}_2(\varphi')\cos(\varphi-\varphi') = \frac{16\Upsilon_a\cos[(\omega_{ka}/v_g-\theta_1/d)d]}{(\Lambda^2+4)^2}, \quad x<x', \tag{A24}
$$

$$
\begin{aligned}
J_{ex} &= \int_{-\infty}^{\infty}d\varphi\int_{-\infty}^{\infty}d\varphi'\tilde{\nu}_1(\varphi)\tilde{\nu}_2(\varphi')\sin|\varphi-\varphi'| = \frac{\Upsilon_a}{(\Lambda^2+4)^2}\left\{\left[8(\omega_{ka}/v_g+\theta_1/d)d + e^{-\frac{2(\omega_{ka}/v_g+\theta_1/d)d}{\Lambda}}\right.\right. \\
&\quad \left.\left.\times 2\Lambda^2(\omega_{ka}/v_g+\theta_0/d)d + 12\Lambda+\Lambda^3\right] + 16\sin[(\omega_{ka}/v_g+\theta_1/d)d]\right\}, \quad x>x',
\end{aligned} \tag{A25}
$$

$$
\begin{aligned}
J'_{ex} &= \int_{-\infty}^{\infty}d\varphi\int_{-\infty}^{\infty}d\varphi'\tilde{\nu}_1(\varphi)\tilde{\nu}_2(\varphi')\sin|\varphi-\varphi'| = \frac{\Upsilon_a}{(\Lambda^2+4)^2}\left\{\left[8(\omega_{ka}/v_g-\theta_1/d)d + e^{-\frac{2(\omega_{ka}/v_g-\theta_1/d)d}{\Lambda}}\right.\right. \\
&\quad \left.\left.\times 2\Lambda^2(\omega_{ka}/v_g-\theta_1/d)d + 12\Lambda+\Lambda^3\right] + 16\sin[(\omega_{ka}/v_g-\theta_1/d)d]\right\}, \quad x<x'.
\end{aligned} \tag{A26}
$$

For the left-incident photon with $z_1(0)\neq 0$ and $z_2(0)=0$, we substitute this equation into $z_1(t)$ as

$$
\begin{aligned}
z_1(t) &= e^{-i\omega_{ka}t}z_1(0) - i\int d\varphi\int d\varphi'[\tilde{\nu}_1(\varphi)+\tilde{\nu}_2(\varphi)]e^{-i\omega_{ka}x/v_g}e^{i\theta(x)} \\
&\quad \times \int d\omega'_{ka}\frac{[\tilde{\nu}_1(\varphi')+\tilde{\nu}_2(\varphi')]e^{i\omega'_{ka}x'/v_g}e^{-i\theta(x')}z_1(0)}{\omega'_{ka}-\omega_e+\Delta_{c1}+\frac{2\Omega_{c1}^2}{\Delta_{c1}}+2i\gamma+i(2\Gamma+2iJ+\Gamma_{ex}+\Gamma'_{ex}+iJ_{ex}+iJ'_{ex})}e^{-i\omega_{ka}t}\int_0^t dt'\tilde{u}_d^{A_c}(t')e^{i(\omega_{ka}-\omega'_{ka})t'},
\end{aligned}
$$

$$
z_1(\infty) = e^{-i\omega_{ka}t}z_1(0)\left\{1 - i\frac{\int d\varphi\int d\varphi'[\tilde{\nu}_1(\varphi)+\tilde{\nu}_2(\varphi)][\tilde{\nu}_1(\varphi')+\tilde{\nu}_2(\varphi')]\cos(\varphi-\varphi')}{\omega_{ka}-\omega_e+\Delta_{c1}+\frac{2\Omega_{c1}^2}{\Delta_{c1}}+2i\gamma+i(2\Gamma+2iJ+\Gamma_{ex}+\Gamma'_{ex}+iJ_{ex}+iJ'_{ex})}\right\}
$$

$$
= e^{-i\omega_{ka}t}z_1(0)\left[1 - \frac{2i(\Gamma+\Gamma'_{ex})}{\omega_{ka}-\omega_e+\Delta_{c1}+\frac{2\Omega_{c1}^2}{\Delta_{c1}}+2i\gamma+i(2\Gamma+2iJ+\Gamma_{ex}+\Gamma'_{ex}+iJ_{ex}+iJ'_{ex})}\right]. \tag{A27}
$$

Therefore, the transmissivity $T_{1\to2}^{\mathrm{eff_c}} \equiv \frac{|z_1(\infty)|^2}{|z_1(0)|^2}$ can be expressed as

$$T_{1\to2}^{\mathrm{eff_c}} = \left| \frac{\delta_{ka} + \Delta_{c1} + \frac{2\Omega_{c1}^2}{\Delta_{c1}} + 2i\gamma - (2J + J_{ex} + J'_{ex}) + i\Gamma_{ex} - i\Gamma'_{ex}}{\delta_{ka} + \Delta_{c1} + \frac{2\Omega_{c1}^2}{\Delta_{c1}} + 2i\gamma + i(2\Gamma + 2iJ + \Gamma_{ex} + \Gamma'_{ex} + iJ_{ex} + iJ'_{ex})} \right|^2. \tag{A28}$$

With the same procedure, for the right-incident photon with $z_1(0) = 0$ and $z_2(0) \neq 0$, we can get the transmissivity $T_{2\to1}^{\mathrm{eff_c}} \equiv \frac{|z_2(\infty)|^2}{|z_2(0)|^2}$ as

$$T_{2\to1}^{\mathrm{eff_c}} = \left| \frac{\delta_{ka} + \Delta_{c1} + \frac{2\Omega_{c1}^2}{\Delta_{c1}} + 2i\gamma - (2J + J_{ex} + J'_{ex}) + i\Gamma'_{ex} - i\Gamma_{ex}}{\delta_{ka} + \Delta_{c1} + \frac{2\Omega_{c1}^2}{\Delta_{c1}} + 2i\gamma + i(2\Gamma + 2iJ + \Gamma_{ex} + \Gamma'_{ex} + iJ_{ex} + iJ'_{ex})} \right|^2. \tag{A29}$$

It is clear that continuous couplings will only change the Lamb shift and effective decay rates, which can be seen from Eqs. (A21)–(A26). Figure 9 shows that even considering the continuous coupling the main results only undergo quantitative changes. Figures 9(a) and 9(b) correspond to the nonchiral and chiral case respectively, indicating that the transmission window and nonreciprocal transmissions still hold.

APPENDIX B: SYMMETRIC FREQUENCY CONVERSION WITH TWO DIFFERENT FIELDS

Similarly, for the model shown in Fig. 4 in the main text, we move to the interaction picture of Hamiltonian in Eq. (10) in the main text as

$$\begin{aligned}\mathcal{H}_{B_k}(t) = &\int dk_a g_a a_{ka} e^{-i\delta_{ka}t} |r_1 g_2\rangle\langle g_1 g_2| \\ &+ \int dk_b g_b b_{kb} e^{-i\delta_{kb}t} e^{ik_b d} |g_1 r_2\rangle\langle g_1 g_2| \\ &+ \Omega_{c1} e^{-i\Delta_{c1}t} |r_1 r_2\rangle\langle r_1 g_2| \\ &+ \Omega_{c2} e^{-i\Delta_{c2}t} e^{i\theta_2} |r_1 r_2\rangle\langle g_1 r_2| + \mathrm{H.c.}\end{aligned} \tag{B1}$$

So the effective Hamiltonian in the interaction picture can be obtained as

$$\begin{aligned}\mathcal{H}_{B_k}^{\mathrm{eff}}(t) \simeq &\frac{g_a^2}{\delta_{ka}} \int dk_a a_{ka} a_{ka}^\dagger |g_1 g_2\rangle\langle g_1 g_2| \\ &+ \frac{g_b^2}{\delta_{kb}} \int dk_b b_{kb} b_{kb}^\dagger |g_1 g_2\rangle\langle g_1 g_2| \\ &- \left(\frac{\Omega_{c1}^2}{\Delta_{c1}} + \frac{\Omega_{c2}^2}{\Delta_{c2}}\right) |r_1 r_2\rangle\langle r_1 r_2| - 2i\gamma |r_1 r_2\rangle\langle r_1 r_2|\end{aligned}$$

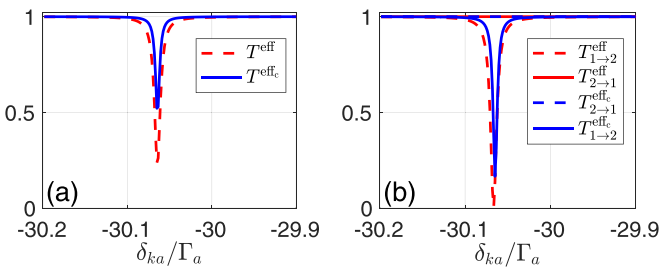

FIG. 9. Transmissivities $T_{1\to2}^{\mathrm{eff}}$ and $T_{2\to1}^{\mathrm{eff}}$ with pointlike couplings and $T_{1\to2}^{\mathrm{eff_c}}$ and $T_{2\to1}^{\mathrm{eff_c}}$ with continuous couplings for (a) $\theta_1 = \theta_2 = 0$ and (b) $\theta_1 = \theta_2 = (2n + 1/2)\pi$ with $\phi_a = \phi_b = (2n + 1/2)\pi$ and $\Lambda = \pi/2$. Other parameters are $\Omega_{c1} = \Gamma_a$, $\Delta_{c1} = 30\Gamma_a$, $\gamma = 10^{-3}\Gamma_a$, $V_6 = 2 \times 10^4 \Gamma_a$, and $\Gamma_a = 1$ MHz.

$$\begin{aligned}&+ \frac{g_a \Omega_{c1}}{\delta_{ka}} \int dk_a a_{ka} e^{-i(\delta_{ka} + \Delta_{c1})t} |r_1 r_2\rangle\langle g_1 g_2| \\ &+ \frac{g_b \Omega_{c2} e^{i\theta_2}}{\delta_{kb}} \int dk_b b_{kb} e^{-i(\delta_{kb} + \Delta_{c2})t} e^{ik_b d} |r_1 r_2\rangle\langle g_1 g_2| \\ &+ \mathrm{H.c.} + \ldots\end{aligned} \tag{B2}$$

and in the Schrödinger picture as

$$\begin{aligned}H_{B_k}^{\mathrm{eff}} = &\left(2\omega_e + V_6 - \frac{\Omega_{c1}^2}{\Delta_{c1}} - \frac{\Omega_{c2}^2}{\Delta_{c2}} - 2i\gamma\right) |r_1 r_2\rangle\langle r_1 r_2| \\ &+ \int dk_a (\omega_{ka} + \omega_{c1}) a_{ka}^\dagger a_{ka} + \int dk_b (\omega_{kb} + \omega_{c2}) b_{kb}^\dagger b_{kb} \\ &+ \int dk_a \xi_a a_{ka} |r_1 r_2\rangle\langle g_1 g_2| \\ &+ \int dk_b \xi_b b_{kb} e^{ik_b d} e^{i\theta_2} |r_1 r_2\rangle\langle g_1 g_2| + \mathrm{H.c.}\end{aligned} \tag{B3}$$

Then the effective Hamiltonian in the real space can be obtained as Eq. (11) in the main text.

Similarly, by solving the eigenequation $H_{B_x}^{\mathrm{eff}} |\tilde{\Psi}_{B_x}\rangle = (\omega_{ka} + \omega_{c1}) |\tilde{\Psi}_{B_x}\rangle$ from Eqs. (11) and (12) in the main text, one can obtain

$$\begin{aligned}(\omega_{ka} + \omega_{c1}) \tilde{\Phi}_{aR}^B(x) &= e^{ik_0 x} \left(\omega_0 - i v_g \frac{\partial}{\partial x}\right) \tilde{\Phi}_{aR}^B(x) e^{-ik_0 x} \\ &\quad + \xi_a \delta(x) \tilde{u}_d^B, \\ (\omega_{ka} + \omega_{c1}) \tilde{\Phi}_{aL}^B(x) &= e^{-ik_0 x} \left(\omega_0 + i v_g \frac{\partial}{\partial x}\right) \tilde{\Phi}_{aL}^B(x) e^{ik_0 x} \\ &\quad + \xi_a \delta(x) \tilde{u}_d^B, \\ (\omega_{ka} + \omega_{c1}) \tilde{\Phi}_{bR}^B(x) &= \left(\omega_0 + \omega_{c2} - \omega_{c1} - i v_g \frac{\partial}{\partial x}\right) \tilde{\Phi}_{bR}^B(x) \\ &\quad + \xi_b e^{i\theta_2} \delta(x - d) \tilde{u}_d^B, \\ (\omega_{ka} + \omega_{c1}) \tilde{\Phi}_{bL}^B(x) &= \left(\omega_0 + \omega_{c2} - \omega_{c1} + i v_g \frac{\partial}{\partial x}\right) \tilde{\Phi}_{bL}^B(x) \\ &\quad + \xi_b e^{i\theta_2} \delta(x - d) \tilde{u}_d^B,\end{aligned}$$

$$(\omega_{ka}+\omega_{c1})\tilde{u}_d^B = (2\omega_e+V_6-2i\gamma)\tilde{u}_d^B + \xi_a\big[\tilde{\Phi}_{aR}^B(0)+\tilde{\Phi}_{aL}^B(0)\big] + \xi_b e^{-i\theta_2}\big[\tilde{\Phi}_{bR}^B(d)+\tilde{\Phi}_{bL}^B(d)\big]. \quad \text{(B4)}$$

Then we substitute the ansatz below (assuming the photon is incident from port 1):

$$\tilde{\Phi}_{aR}^B = e^{ik_a x}\big[\Theta(-x)+s_{1\to2}^{\text{eff}}\Theta(x)\big],$$
$$\tilde{\Phi}_{aL}^B = e^{-ik_a x}\big[s_{1\to1}^{\text{eff}}\Theta(-x)\big],$$
$$\tilde{\Phi}_{bR}^B = e^{ik_b x}\big[s_{1\to4}^{\text{eff}}\Theta(x-d)\big],$$
$$\tilde{\Phi}_{bL}^B = e^{-ik_b x}\big[s_{1\to3}^{\text{eff}}\Theta(-x+d)\big] \quad \text{(B5)}$$

and we can calculate the reflectivity, transmissivity, and backward and forward conversion efficiencies as in Eq. (13) in the main text.

APPENDIX C: ASYMMETRIC FREQUENCY CONVERSION WITH TWO DIFFERENT FIELDS

For the model shown in Fig. 6 in the main text, the Hamiltonian in the interaction picture based on Eq. (14) can be expressed as

$$\mathcal{H}_{C_k}(t) = \int dk_a g_a a_{ka} e^{-i\delta_{ka}t}(|r_1g_2\rangle\langle g_1g_2| + e^{ik_a d}|g_1r_2\rangle\langle g_1g_2|) + \int dk_b g_b b_{kb} e^{-i\delta_{kb}t}(|r_1g_2\rangle\langle g_1g_2| + e^{ik_b d}|g_1r_2\rangle\langle g_1g_2|) + \Omega_{c1}e^{-i\Delta_{c1}t}(|r_1r_2\rangle\langle r_1g_2| + e^{i\theta_1}|r_1r_2\rangle\langle g_1r_2|) + \Omega_{c2}e^{-i\Delta_{c2}t}(|r_1r_2\rangle\langle r_1g_2| + e^{i\theta_2}|r_1r_2\rangle\langle g_1r_2|) + \text{H.c.} \quad \text{(C1)}$$

With the same procedure, the effective Hamiltonian in the interaction picture can be obtained as

$$\begin{aligned}\mathcal{H}_{C_k}^{\text{eff}}(t) \simeq{}& \frac{2g_a^2}{\delta_{ka}}\int dk_a a_{ka}a_{ka}^\dagger|g_1g_2\rangle\langle g_1g_2| + \frac{2g_b^2}{\delta_{kb}}\int dk_b b_{kb}b_{kb}^\dagger|g_1g_2\rangle\langle g_1g_2| + \frac{2g_ag_b}{\delta_{ka}}\int dk_a a_{ka}b_{kb}^\dagger|g_1g_2\rangle\langle g_1g_2|e^{i(\delta_{kb}-\delta_{ka})t} \\ &+ \frac{2g_ag_b}{\delta_{kb}}\int dk_b b_{kb}a_{ka}^\dagger|g_1g_2\rangle\langle g_1g_2|e^{i(\delta_{ka}-\delta_{kb})t} - \frac{2\Omega_{c1}^2}{\Delta_{c1}}|r_1r_2\rangle\langle r_1r_2| - \frac{2\Omega_{c2}^2}{\Delta_{c2}}|r_1r_2\rangle\langle r_1r_2| \\ &- \frac{2\Omega_{c1}\Omega_{c2}}{\Delta_{c1}}|r_1r_2\rangle\langle r_1r_2|e^{i(\Delta_{c1}-\Delta_{c2})t} - \frac{2\Omega_{c1}\Omega_{c2}}{\Delta_{c2}}|r_1r_2\rangle\langle r_1r_2|e^{i(\Delta_{c2}-\Delta_{c1})t} \\ &+ \frac{g_a\Omega_{c1}e^{i\theta_1}}{\delta_{ka}}\int dk_a a_{ka}e^{-i(\delta_{ka}+\Delta_{c1})t}(1+e^{ik_a d})|r_1r_2\rangle\langle g_1g_2| + \frac{g_b\Omega_{c2}e^{i\theta_2}}{\delta_{kb}}\int dk_b b_{kb}e^{-i(\delta_{kb}+\Delta_{c2})t}(1+e^{ik_b d})|r_1r_2\rangle\langle g_1g_2| \\ &+ \frac{g_b\Omega_{c1}e^{i\theta_1}}{\delta_{kb}}\int dk_b b_{kb}e^{-i(\delta_{kb}+\Delta_{c1})t}(1+e^{ik_b d})|r_1r_2\rangle\langle g_1g_2| + \frac{g_a\Omega_{c2}e^{i\theta_2}}{\delta_{ka}}\int dk_a kbe^{-i(\delta_{ka}+\Delta_{c2})t}(1+e^{ik_a d})|r_1r_2\rangle\langle g_1g_2| \\ &+ \text{H.c.} + \ldots. \end{aligned} \quad \text{(C2)}$$

Besides omitting the terms related to the single-excitation states done as the last two models, the terms with $e^{\pm i(\Delta_{c1}+\delta_{kb})t}$ and $e^{\pm i(\Delta_{c2}+\delta_{ka})t}$ can also be discarded since they are regarded as high-frequency oscillation terms if assuming $|\Delta_{c1}+\delta_{kb}| \gg g_b\Omega_{c1}/\delta_{kb}$ and $|\Delta_{c2}+\delta_{ka}| \gg g_a\Omega_{c2}/\delta_{ka}$, while taking $\Delta_{c1}+\delta_{ka} \simeq 0$ and $\Delta_{c2}+\delta_{kb} \simeq 0$. Then, in the same way, after transferring the Hamiltonian to the Schrödinger picture, one can obtain the real-space effective Hamiltonian as Eq. (15) in the main text.

Similarly, by solving the eigenequation one can obtain

$$\begin{aligned}(\omega_{ka}+\omega_{c1})\tilde{\Phi}_{aR}^C(x) &= e^{ik_0x}\Big(\omega_0 - iv_g\frac{\partial}{\partial x}\Big)\tilde{\Phi}_{aR}^C(x)e^{-ik_0x} + [\xi_a\delta(x)+\xi_a e^{i\theta_1}\delta(x-d)]\tilde{u}_d^C, \\ (\omega_{ka}+\omega_{c1})\tilde{\Phi}_{aL}^C(x) &= e^{-ik_0x}\Big(\omega_0 + iv_g\frac{\partial}{\partial x}\Big)\tilde{\Phi}_{aL}^C(x)e^{ik_0x} + [\xi_a\delta(x)+\xi_a e^{i\theta_1}\delta(x-d)]\tilde{u}_d^C, \\ (\omega_{ka}+\omega_{c1})\tilde{\Phi}_{bR}^C(x) &= e^{ik_0x}\Big(\omega_0+\omega_{c2}-\omega_{c1} - iv_g\frac{\partial}{\partial x}\Big)\tilde{\Phi}_{bR}^C(x)e^{-ik_0x} + [\xi_b\delta(x)+\xi_b e^{i\theta_2}\delta(x-d)]\tilde{u}_d^C, \\ (\omega_{ka}+\omega_{c1})\tilde{\Phi}_{bL}^C(x) &= e^{-ik_0x}\Big(\omega_0+\omega_{c2}-\omega_{c1} + iv_g\frac{\partial}{\partial x}\Big)\tilde{\Phi}_{bL}^C(x)e^{ik_0x} + [\xi_b\delta(x)+\xi_b e^{i\theta_2}\delta(x-d)]\tilde{u}_d^C, \\ (\omega_{ka}+\omega_{c1})\tilde{u}_d^C &= (2\omega_e+V_6-2i\gamma)\tilde{u}_d^C + \xi_a\big[\tilde{\Phi}_{aR}^C(0)+\tilde{\Phi}_{aL}^C(0)\big] + \xi_a e^{-i\theta_1}\big[\tilde{\Phi}_{aR}^C(d)+\tilde{\Phi}_{aL}^C(d)\big] \\ &\quad + \xi_b\big[\tilde{\Phi}_{bR}^C(0)+\tilde{\Phi}_{bL}^C(0)\big] + \xi_b e^{-i\theta_2}\big[\tilde{\Phi}_{bR}^C(d)+\tilde{\Phi}_{bL}^C(d)\big]. \end{aligned} \quad \text{(C3)}$$

We substitute the new ansatz below with two coupling points of each waveguide mode (assuming the photon is incident from port 1):

$$\begin{aligned}\tilde{\Phi}_{aR}^C &= e^{ik_a x}\big\{\Theta(-x)+C_1^{\text{eff}}[\Theta(x)-\Theta(x-d)]+p_{1\to2}\Theta(x-d)\big\}, \\ \tilde{\Phi}_{aL}^C &= e^{-ik_a x}\big\{p_{1\to1}\Theta(-x)+C_2^{\text{eff}}[\Theta(x)-\Theta(x-d)]\big\}, \\ \tilde{\Phi}_{bR}^C &= e^{ik_b x}\big\{C_3^{\text{eff}}[\Theta(x)-\Theta(x-d)]+p_{1\to4}\Theta(x-d)\big\}, \\ \tilde{\Phi}_{bL}^C &= e^{-ik_b x}\big\{p_{1\to3}\Theta(-x)+C_4^{\text{eff}}[\Theta(x)-\Theta(x-d)]\big\}. \end{aligned} \quad \text{(C4)}$$

The reflectivity, transmissivity, and backward and forward conversion efficiencies can be calculated as in Eq. (16) in the main text.

[1] M. Saffman, T. G. Walker, and K. Mølmer, Quantum information with Rydberg atoms, Rev. Mod. Phys. **82**, 2313 (2010).

[2] M. Morgado and S. Whitlock, Quantum simulation and computing with Rydberg-interacting qubits, AVS Quantum Sci. **3**, 023501 (2021).

[3] I. Cong, H. Levine, A. Keesling, D. Bluvstein, S.-T. Wang, and M. D. Lukin, Hardware-efficient, fault-tolerant quantum computation with Rydberg atoms, Phys. Rev. X **12**, 021049 (2022).

[4] M. D. Lukin, M. Fleischhauer, R. Cote, L. M. Duan, D. Jaksch, J. I. Cirac, and P. Zoller, Dipole blockade and quantum information processing in mesoscopic atomic ensembles, Phys. Rev. Lett. **87**, 037901 (2001).

[5] D. Petrosyan and K. Mølmer, Deterministic free-space source of single photons using Rydberg atoms, Phys. Rev. Lett. **121**, 123605 (2018).

[6] F. Ripka, H. Kübler, R. Löw, and T. Pfau, A room-temperature single-photon source based on strongly interacting Rydberg atoms, Science **362**, 446 (2018).

[7] D. P. Ornelas-Huerta, A. N. Craddock, E. A. Goldschmidt, A. J. Hachtel, Y. Wang, P. Bienias, A. V. Gorshkov, S. L. Rolston, and J. V. Porto, On-demand indistinguishable single photons from an efficient and pure source based on a Rydberg ensemble, Optica **7**, 813 (2020).

[8] D. Møller, L. B. Madsen, and K. Mølmer, Quantum gates and multiparticle entanglement by Rydberg excitation blockade and adiabatic passage, Phys. Rev. Lett. **100**, 170504 (2008).

[9] D. Tiarks, S. Schmidt-Eberle, T. Stolz, G. Rempe, and S. Dürr, A photon-photon quantum gate based on Rydberg interactions, Nat. Phys. **15**, 124 (2019).

[10] K. McDonnell, L. F. Keary, and J. D. Pritchard, Demonstration of a quantum gate using electromagnetically induced transparency, Phys. Rev. Lett. **129**, 200501 (2022).

[11] D. D. Bhaktavatsala Rao and K. Mølmer, Dark entangled steady states of interacting Rydberg atoms, Phys. Rev. Lett. **111**, 033606 (2013).

[12] H. Levine, A. Keesling, A. Omran, H. Bernien, S. Schwartz, A. S. Zibrov, M. Endres, M. Greiner, V. Vuletić, and M. D. Lukin, High-fidelity control and entanglement of Rydberg-atom qubits, Phys. Rev. Lett. **121**, 123603 (2018).

[13] I. S. Madjarov, J. P. Covey, A. L. Shaw, J. Choi, A. Kale, A. Cooper, H. Pichler, V. Schkolnik, J. R. Williams, and M. Endres, High-fidelity entanglement and detection of alkaline-earth Rydberg atoms, Nat. Phys. **16**, 857 (2020).

[14] P.-F. Sun, Y. Yu, Z.-Y. An, J. Li, C.-W. Yang, X.-H. Bao, and J.-W. Pan, Deterministic time-bin entanglement between a single photon and an atomic ensemble, Phys. Rev. Lett. **128**, 060502 (2022).

[15] J. Zeiher, J.-Y. Choi, A. Rubio-Abadal, T. Pohl, R. van Bijnen, I. Bloch, and C. Gross, Coherent many-body spin dynamics in a long-range interacting Ising chain, Phys. Rev. X **7**, 041063 (2017).

[16] H. Kim, Y. Park, K. Kim, H.-S. Sim, and J. Ahn, Detailed balance of thermalization dynamics in Rydberg-atom quantum simulators, Phys. Rev. Lett. **120**, 180502 (2018).

[17] Y.-T. Chen, L. Du, Y. Zhang, L. Guo, J.-H. Wu, M. Artoni, and G. C. La Rocca, Giant-atom effects on population and entanglement dynamics of Rydberg atoms in the optical regime, Phys. Rev. Res. **5**, 043135 (2023).

[18] A. F. Kockum, Quantum optics with giant atoms: The first five years, in *Mathematics for Industry* (Springer, New York, 2021), pp. 125–146.

[19] M. V. Gustafsson, T. Aref, A. F. Kockum, M. K. Ekström, G. Johansson, and P. Delsing, Propagating phonons coupled to an artificial atom, Science **346**, 207 (2014).

[20] G. Andersson, B. Suri, L. Guo, T. Aref, and P. Delsing, Nonexponential decay of a giant artificial atom, Nat. Phys. **15**, 1123 (2019).

[21] B. Kannan, M. Ruckriegel, D. Campbell, A. F. Kockum, J. Braumüller, D. Kim, M. Kjaergaard, P. Krantz, A. Melville, B. M. Niedzielski, A. Vepsäläinen, R. Winik, J. Yoder, F. Nori, T. P. Orlando, S. Gustavsson, and W. D. Oliver, Waveguide quantum electrodynamics with superconducting artificial giant atoms, Nature (London) **583**, 775 (2020).

[22] A. M. Vadiraj, Andreas Ask, T. G. McConkey, I. Nsanzineza, C. W. Sandbo Chang, A. F. Kockum, and C. M. Wilson, Engineering the level structure of a giant artificial atom in waveguide quantum electrodynamics, Phys. Rev. A **103**, 023710 (2021).

[23] S. Longhi, Photonic simulation of giant atom decay, Opt. Lett. **45**, 3017 (2020).

[24] Z. Q. Wang, Y. P. Wang, J. Yao, R. C. Shen, W. J. Wu, J. Qian, J. Li, S. Y. Zhu, and J. Q. You, Giant spin ensembles in waveguide magnonics, Nat. Commun. **13**, 7580 (2022).

[25] A. Frisk Kockum, P. Delsing, and G. Johansson, Designing frequency-dependent relaxation rates and Lamb shifts for a giant artificial atom, Phys. Rev. A **90**, 013837 (2014).

[26] Q. Y. Cai and W. Z. Jia, Coherent single-photon scattering spectra for a giant-atom waveguide-QED system beyond the dipole approximation, Phys. Rev. A **104**, 033710 (2021).

[27] Q.-Y. Qiu, Y. Wu, and X.-Y. Lü, Collective radiance of giant atoms in non-Markovian regime, Sci. China Phys. Mech. Astron. **66**, 224212 (2023).

[28] L. Guo, A. L. Grimsmo, A. F. Kockum, M. Pletyukhov, and G. Johansson, Giant acoustic atom: A single quantum system with a deterministic time delay, Phys. Rev. A **95**, 053821 (2017).

[29] A. F. Kockum, G. Johansson, and F. Nori, Decoherence-free interaction between giant atoms in waveguide quantum electrodynamics, Phys. Rev. Lett. **120**, 140404 (2018).

[30] A. Carollo, D. Cilluffo, and F. Ciccarello, Mechanism of decoherence-free coupling between giant atoms, Phys. Rev. Res. **2**, 043184 (2020).

[31] A. Soro, and A. F. Kockum, Chiral quantum optics with giant atoms, Phys. Rev. A **105**, 023712 (2022).

[32] A. C. Santos and R. Bachelard, Generation of maximally entangled long-lived states with giant atoms in a waveguide, Phys. Rev. Lett. **130**, 053601 (2023).

[33] R. Mitsch, C. Sayrin, B. Albrecht, P. Schneeweiss, and A. Rauschenbeutel, Quantum state-controlled directional spontaneous emission of photons into a nanophotonic waveguide, Nat. Commun. **5**, 5713 (2014).

[34] J. Petersen, J. Volz, and A. Rauschenbeutel, Chiral nanophotonic waveguide interface based on spin-orbit interaction of light, Science **346**, 67 (2014).

[35] K. Y. Bliokh and F. Nori, Transverse and longitudinal angular momenta of light, Phys. Rep. **592**, 1 (2015).

[36] M. Bello, G. Platero, J. I. Cirac, and A. González-Tudela, Unconventional quantum optics in topological waveguide QED, Sci. Adv. **5**, eaaw0297 (2019).

[37] E. Kim, X. Zhang, V. S. Ferreira, J. Banker, J. K. Iverson, A. Sipahigil, M. Bello, A. González-Tudela, M. Mirhosseini, and O. Painter, Quantum electrodynamics in a topological waveguide, Phys. Rev. X **11**, 011015 (2021).

[38] X. Wang and H.-R. Li, Chiral quantum network with giant atoms, Quantum Sci. Technol. **7**, 035007 (2022).

[39] Y.-T. Chen, L. Du, L. Guo, Z. Wang, Y. Zhang, Y. Li, and J. H. Wu, Nonreciprocal and chiral single-photon scattering for giant atoms, Commun. Phys. **5**, 215 (2022).

[40] L. Du, Y. Zhang, J.-H. Wu, A. F. Kockum, and Y. Li, Giant atoms in synthetic frequency dimensions, Phys. Rev. Lett. **128**, 223602 (2022).

[41] C. Joshi, F. Yang, and M. Mirhosseini, Resonance fluorescence of a chiral artificial atom, Phys. Rev. X **13**, 021039 (2023).

[42] C. Gonzalez-Ballestero, E. Moreno, F. J. Garcia-Vidal, and A. Gonzalez-Tudela, Nonreciprocal few-photon routing schemes based on chiral waveguide-emitter couplings, Phys. Rev. A **94**, 063817 (2016).

[43] C. H. Yan, Y. Li, H. D. Yuan, and L. F. Wei, Targeted photonic routers with chiral photon-atom interactions, Phys. Rev. A **97**, 023821 (2018).

[44] K. Xia, G. Lu, G. Lin, Y. Cheng, Y. Niu, S. Gong, and J. Twamley, Reversible nonmagnetic single-photon isolation using unbalanced quantum coupling, Phys. Rev. A **90**, 043802 (2014).

[45] Y. You, Y. Hu, G. Lin, Y. Qi, Y. Niu, and S. Gong, Quantum nonreciprocity based on electromagnetically induced transparency in chiral quantum-optical systems, Phys. Rev. A **103**, 063706 (2021).

[46] M. Bradford, K. C. Obi, and J.-T. Shen, Efficient single-photon frequency conversion using a sagnac interferometer, Phys. Rev. Lett. **108**, 103902 (2012).

[47] Z. H. Wang, L. Zhou, Y. Li, and C. P. Sun, Controllable single-photon frequency converter via a one-dimensional waveguide, Phys. Rev. A **89**, 053813 (2014).

[48] W. Z. Jia, Y. W. Wang, and Y.-X. Liu, Efficient single-photon frequency conversion in the microwave domain using superconducting quantum circuits, Phys. Rev. A **96**, 053832 (2017).

[49] L. Du, and Y. Li, Single-photon frequency conversion via a giant Λ-type atom, Phys. Rev. A **104**, 023712 (2021).

[50] J.-T. Shen and S. Fan, Coherent single photon transport in a one-dimensional waveguide coupled to superconducting quantum bits, Phys. Rev. Lett. **95**, 213001 (2005).

[51] J.-T. Shen and S. Fan, Theory of single-photon transport in a single-mode waveguide. I. Coupling to a cavity containing a two-level atom, Phys. Rev. A **79**, 023837 (2009).

[52] W. Zhao and Z. Wang, Single-photon scattering and bound states in an atom-waveguide system with two or multiple coupling points, Phys. Rev. A **101**, 053855 (2020).

[53] X.-L. Yin, Y.-H. Liu, J.-F. Huang, and J.-Q. Liao, Single-photon scattering in a giant-molecule waveguide-QED system, Phys. Rev. A **106**, 013715 (2022).

[54] Z. Liao, X. Zeng, H. Nha, and M. S. Zubairy, Photon transport in a one-dimensional nanophotonic waveguide QED system, Phys. Scr. **91**, 063004 (2016).

[55] R. N. Bracewell, *The Fourier Transform and its Applications* (McGraw-Hill, New York, 2007).

[56] E. Brion, L. H. Pedersen, and K. Mølmer, Adiabatic elimination in a lambda system, J. Phys. A **40**, 1033 (2007).

[57] D. Yan, J.-W. Gao, Q.-Q. Bao, H. Yang, H. Wang, and J.-H. Wu, Electromagnetically induced transparency in a five-level Λ system dominated by two-photon resonant transitions, Phys. Rev. A **83**, 033830 (2011).

[58] A. L. de Oliveira, M. W. Mancini, V. S. Bagnato, and L. G. Marcassa, Measurement of Rydberg-state lifetimes using cold trapped atoms, Phys. Rev. A **65**, 031401(R) (2002).

[59] M. S. Safronova and U. I. Safronova, Critically evaluated theoretical energies, lifetimes, hyperfine constants, and multipole polarizabilities in ^{87}Rb, Phys. Rev. A **83**, 052508 (2011).

[60] M. Archimi, C. Simonelli, L. Di Virgilio, A. Greco, M. Ceccanti, E. Arimondo, D. Ciampini, I. I. Ryabtsev, I. I. Beterov, and O. Morsch, Measurements of single-state and state-ensemble lifetimes of high-lying Rb Rydberg levels, Phys. Rev. A **100**, 030501(R) (2019).

[61] K. Wongcharoenbhorn, C. Koller, T. M. Fromhold, and W. Li, Casimir-Polder interactions of *S*-state Rydberg atoms with graphene, Phys. Rev. A **107**, 043308 (2023).

[62] T.-H. Chang, B. M. Fields, M. E. Kim, and C.-L. Hung, Microring resonators on a suspended membrane circuit for atom–light interactions, Optica **6**, 1203 (2019).